Transcriptomic analysis in zebrafish larvae identifies iron-dependent mitochondrial dysfunction as a possible key event of NAFLD progression induced by benzo[a]pyrene/ethanol co-exposure

Muhammad Imran, Frédéric Chalmel, Odile Sergent, Bertrand Evrard, Hélène Le Mentec, Antoine Legrand, Aurélien Dupont, Maëlle Bescher, Simon Bucher, Bernard Fromenty, et al.

Transcriptomic analysis in zebrafish larvae identifies iron-dependent mitochondrial dysfunction as a possible key event of NAFLD progression induced by benzo[a]pyrene/ethanol co-exposure

Muhammad Imran[1 $], Frédéric Chalmel[1], Odile Sergent[1], Bertrand Evrard[1], Hélène Le Mentec[1], Antoine Legrand[1], Aurélien Dupont[2], Maëlle Bescher[1], Simon Bucher[3], Bernard Fromenty[3], Laurence Huc[4], Lydie Sparfel[1] *, Dominique Lagadic-Gossmann[1] *, Normand Podechard[1] *#

[1] Univ Rennes, Inserm, EHESP, Irset (Institut de recherche en santé environnement et travail) – UMR_S 1085, F-35000 Rennes, France

[2] Univ Rennes, Biosit – UMS 3480, US_S 018, F-35000 Rennes, France

[3] Univ Rennes, Inserm, Inra, Institut NUMECAN (Nutrition Metabolisms and Cancer)–UMR_S 1241, and UMR_A 1341, 35000 Rennes, France

[4] Toxalim (Research Centre in Food Toxicology), Université de Toulouse, INRA, ENVT, INP-Purpan, UPS, 31027 Toulouse, France

 # Corresponding author:

Normand Podechard, norman.podechard@univ-rennes1.fr (ORCID ID: 0000-0002-2638-3180) ; UMR Inserm U1085 / IRSET, University of Rennes 1, Faculty of Pharmacy, 2 av. Pr. Léon Bernard, 35043 RENNES cedex, France

$ Present address: Iqra University, Karachi, Pakistan

*** Co-last authors**

Abstract

Non-alcoholic fatty liver disease (NAFLD) is a worldwide epidemic for which environmental contaminants are increasingly recognized as important etiological factors. Among them, the combination of benzo[a]pyrene (B[a]P), a potent environmental carcinogen, with ethanol, was shown to induce the transition of steatosis towards steatohepatitis. However, the underlying mechanisms involved remain to be deciphered. In this context, we used high-fat diet fed zebrafish model, in which we previously observed progression of steatosis to a steatohepatitis-like state following a 7 days-co-exposure to 43 mM ethanol and 25 nM B[a]P. Transcriptomic analysis highlighted the potent role of mitochondrial dysfunction, alterations in heme and iron homeostasis, involvement of aryl hydrocarbon receptor (AhR) signaling and oxidative stress. Most of these mRNA dysregulations were validated by RT-qPCR. Moreover, similar changes were observed using a human *in vitro* hepatocyte model, HepaRG cells. The mitochondria structural and functional alterations were confirmed by transmission electronic microscopy and Seahorse technology, respectively. Involvement of AhR signaling was evidenced by using *in vivo* an AhR antagonist, CH223191 and *in vitro* in AhR-knock-out HepaRG cells. Furthermore, as co-exposure was found to increase the levels of both heme and hemin, we investigated if mitochondrial iron could induce oxidative stress. We found that mitochondrial labile iron content was raised in toxicant-exposed larvae. This increase was prevented by the iron chelator, deferoxamine, which also inhibited liver co-exposure toxicity. Overall, these results suggest that the increase in mitochondrial iron content induced by B[a]P/ethanol co-exposure causes mitochondrial dysfunction that contributes to the pathological progression of NAFLD.

Keyword :

NAFLD, iron homeostasis, mitochondrial dysfunction, AhR, B[a]P, ethanol, zebrafish

Abbreviations:

AhR: Aryl hydrocarbon receptor, AhR-KO: AhR knock out , AMEN: Annotation, Mapping, Expression and Network suite of tools, ANOVA: One-way analysis of variance, B[a]P: Benzo[a]pyrene, CREEA: Comité Rennais d'Ethique en matière d'Expérimentation Animale, DMSO: Dimethyl sulfoxide, DPF: Days post-fertilization, FA: Fatty acids, FCCP: Carbonyl cyanide-p-trifluoro methoxyphenyl hydrazone, GEO: Expression Omnibus, GO: Gene ontology, GOEA: Gene ontology enrichment analysis, HES: Hematoxylin-Eosin-Safranin; HFD: High fat diet, HO1: Heme oxygenase 1, IARC: International Agency for Research on Cancer, IPA: Ingenuity pathway analysis, KEGG: Kyoto Encyclopedia of Genes and Genomes, NADP: Nicotinamide adenine dinucleotide phosphate, NAFLD: Alcoholic fatty liver disease, NaN_3: Sodium azide, NASH: Non-alcoholic steatohepatitis, NOS: Reactive nitrogen species, OCR: Oxygen consumption rate, OXPHOS: Oxidative phosphorylation, PAH: Polycyclic aryl hydrocarbon, PBS: Phosphate-buffered saline, PMT: Photomultiplier tube, ROS: Reactive oxygen species, SEM: Standard error of the mean, T2DM: Type 2 Diabetes mellitus, TAFLD: Toxicant-Associated Fatty Liver Diseases, TASH: Toxicant-Associated Steatohepatitis, TCDD: 2,3,7,8-Tetrachlorodibenzo-p-dioxin, TEM: Transmission electronic microscopy.

1. Introduction

Non-alcoholic fatty liver disease (NAFLD) is now well recognized as a growing worldwide epidemic, responsible for an increasing number of chronic liver diseases and consecutive mortality (Younossi 2019). NAFLD covers a large panel of liver diseases, starting from liver steatosis to its pathological progression into non-alcoholic steatohepatitis (NASH), with possible evolution towards severe and irreversible complications such as cirrhosis and/or hepatocellular carcinoma (Fazel et al. 2016). The global prevalence of NAFLD is around 25% of general population all over the world, while for NASH, it reaches between 3 to 5% (Younossi 2019). It should be noted that some subpopulations are particularly affected by NAFLD, notably patients exhibiting metabolic diseases such as type 2 Diabetes mellitus (T2DM) and obesity, in which NAFLD prevalence could rise to 60 or 90% respectively (Younossi 2019). Beyond principal etiological factors of NAFLD, *i.e.* metabolic diseases like obesity and T2DM, there are several others like dietary habits (including moderate/heavy alcohol consumption), genetic polymorphisms, gender, epigenetic factors as well as environmental factors (Younossi 2019). In this concern, the role of these latter factors has gained interest during last years, leading to the concept of TAFLD and TASH (Toxicant-Associated Fatty Liver Diseases and Toxicant-Associated Steatohepatitis) as proposed by Cave and co-workers (Joshi-Barve et al. 2015; Wahlang et al. 2019). In line with this, several pollutants, including ligands of aryl hydrocarbon receptor (AhR), have thus been shown to induce steatosis or favor its pathological progression (Wahlang et al. 2019).

In this context, another challenging concern is the impact of chemical mixtures on NAFLD particularly in high-risk populations such as people already presenting fatty liver. In

that way, we have previously demonstrated that co-exposure to benzo[a]pyrene (B[a]P), the reference molecule of the PAH (polycyclic aryl hydrocarbon) family, in combination with a well-known hepatotoxicant, ethanol, induces the transition of steatosis towards a steatohepatitis—like state both *in vitro* and *in vivo* (Bucher et al. 2018b; Bucher et al. 2018a; Imran et al. 2018; Tête et al. 2018). B[a]P, a widespread environmental contaminant, is a potent carcinogen to human (classified in group 1 by IARC), and a strong AhR ligand (Das and Bhutia 2018; Hardonnière et al. 2017; International Agency for Research on Cancer (IARC) 2012). B[a]P is a pollutant formed, like other PAHs, during incomplete combustion of organic compounds. Human exposure to B[a]P, excluding smoking or occupational exposure, is mainly food-borne notably with barbecued/grilled/broiled/smoked meats, grain and cereals (Das and Bhutia 2018; International Agency for Research on Cancer (IARC) 2012). Most of the toxic effects of B[a]P depend on its bioactivation by cytochrome P450s (CYP), which mainly occurs in liver. This thus explains the adverse effects of this pollutant on this organ through several mechanisms including oxidative stress, genotoxicity, mitochondrial dysfunction, cell death (Das and Bhutia 2018; Hardonnière et al. 2016; International Agency for Research on Cancer (IARC) 2012; Tekpli et al. 2010; Uno et al. 2018). B[a]P, as other toxicants, has been implicated in NAFLD development and progression (Wahlang et al. 2019). Regarding the impact of B[a]P/ethanol co-exposure, frequently observed in population, on steatosis progression, we recently evidenced several mechanisms using *in vitro* models such as the human hepatic cell line, HepaRG (Bucher et al. 2018a; Tête et al. 2018). However, the underlying mechanisms involved in the exacerbation of NAFLD upon such a co-exposure remain to be deciphered *in vivo*.

To this aim, we used an *in vivo* model of zebrafish larvae to have an integrative model in which the complexity and variety of cell and organ interactions are present and relevant to human NAFLD pathogenesis (Chu and Sadler 2009; Goessling and Sadler 2015; Schlegel 2012). In addition to technical advantages like small size and transparency, zebrafish larvae also present broad similarities with humans concerning liver functions and sensitivity toward xenobiotics and alcohol (metabolism, toxicity, cellular and transcriptomic responses) (Driessen et al. 2014; Driessen et al. 2013; Goessling and Sadler 2015; Goldstone et al. 2010). Besides, the full machinery for B[a]P metabolism exists in zebrafish notably with the expression of *ahr2*, the ligand-activated ortholog of AhR (Goodale et al. 2012). For the present study, we used a recently established zebrafish larvae model of high fat diet (HFD)-induced steatosis in which we observed steatosis progression following a 7 days-co-exposure to low doses of ethanol and B[a]P, respectively 43 mM and 25 nM (Bucher et al. 2018b; Imran et al. 2018). In order to elucidate the mechanisms involved in the pathological progression of steatosis induced upon B[a]P/ethanol co-exposure in HFD-zebrafish larvae, a transcriptomic approach was performed in the present study. We identified and confirmed by RT-qPCR, disruptions of key processes, *i.e.* mitochondrial dysfunctions, alterations of heme and iron metabolism, AhR signaling and oxidative stress, which were then more deeply investigated. Our main results strongly suggest the involvement of a mitochondrial overload of labile iron as a key event in the liver disease progression upon B[a]P/ethanol co-exposure. Furthermore, these effects were prevented by the common iron-chelating drug, deferoxamine.

2. Materials and Methods

Details for all Materials and methods are available in supplementary material (File S1).

3. Results

3.1. Transcriptomic analysis identifies heme homeostasis and mitochondrial dysfunction as potential events of liver disease progression in B[a]P/ethanol co-exposed HFD zebrafish larvae

In order to decipher the cellular mechanisms involved in the progression of liver steatosis in HFD zebrafish larvae co-exposed to B[a]P and ethanol, we performed a transcriptomic analysis based on affymetrix microarray technology (GeneChip™ Zebrafish Gene 1.0 ST Array). Briefly, HFD zebrafish larvae were chronically exposed to 43 mM ethanol and/or to 25 nM B[a]P from 5 dpf until 12 dpf (doses chosen in rationale to human level exposure and already shown to induce progression of steatosis in our zebrafish model (Bucher et al. 2018b; Imran et al. 2018)). From transcriptomic analysis, 525 differentially expressed genes (DEGs) were found after co-exposure compared to control. Those genes were further partitioned into 8 expression clusters (termed P1-P8) organized in two broad expression patterns corresponding to up-regulated (315 DEGs, corresponding to P1-4) and down-regulated (210 DEGs, P5-8) genes (see supplementary Table S1 for all data) (Figure 1a and b). The functional analysis revealed that up-regulated genes were significantly associated with porphyrin metabolism and mitochondria (GO:0006787 porphyrin-containing compound catabolic process; GO:0031966 mitochondrial membrane; KEGG:00860 porphyrin and chlorophyll metabolism) (Figure 1c). Interestingly, these terms were also found to be significantly enriched in the 4 up-regulated clusters (P1-4) thereby indicating that the observed alterations were not just due to one toxicant; rather both B[a]P and ethanol were effective, particularly when used in combination (Figure 1b). Regarding down-regulated genes, most of the terms appeared to be related to

immunity (for example: GO:0060333 IFNg-mediated signaling pathways; GO:0043312 neutrophil degranulation or GO:0030670 phagocytic vesicle membrane) (Figure 1b). To improve relevance of findings regarding human health, we performed an Ingenuity Pathways Analysis (IPA) following conversion of the 525 zebrafish DEGs into 259 human homologs (supplementary Table S2); several terms were then presented for canonical pathways, toxicity lists and toxicity functions (summary presented in supplementary Table S3; full results are provided in supplementary Table S4). In line with the functional analysis performed in AMEN, the selected terms highlight mitochondria dysfunction and alterations in heme homeostasis, involvement of AhR signaling and oxidative stress for canonical pathways and toxicity lists (supplementary Table S3). Finally, analysis of toxicity functions markedly outlined the impact of B[a]P/ethanol co-exposure on liver diseases (supplementary Table S3) in agreement with our previous work (Bucher et al. 2018b; Imran et al. 2018; Tête et al. 2018).

3.2. Validation and investigation by RT-qPCR of molecular dysregulations induced by co-exposure

In order to validate the microarray results from our zebrafish model, we performed RT-qPCR assays on zebrafish samples (Figure 2a to 2c) (Note that for all genes studied by RT-qPCR and presented by abbreviation, full names could be found in the supplementary file S5 with primer information). One of the main processes identified through the transcriptomic analysis in *in vivo* steatosis progression upon B[a]P/ethanol co-exposure appeared to be mitochondrial dysfunction. In fact, this was in line with our recent work realized *in vitro* in human HepaRG cell line (Bucher et al. 2018a). In order to get further insight into mitochondrial dysfunction, especially *in vivo*, we decided to perform RT-qPCR on several target genes selected either from our transcriptomic screening or according to their role in mitochondrial function (Figure 2a).

Most of the transcripts found to be dysregulated in our microarray (indicated by an arrow in Figure 2a to 2c), were validated by RT-qPCR with significant changes (22 transcripts out of the 25 found in microarray). Among mitochondria-related genes, the expression of several transporters of metabolites (*abcg2a*, *slc25a25a*, *slc25a47a*, *slc25a48* and *tspo*) was induced, thus suggesting alterations of mitochondrial metabolism (Figure 2a). Interestingly, *abcg2a* and *tspo* are also known to be involved in heme homeostasis. Regarding genes related to electron transport chain, mitochondrial respiration and ATP production, several were found to be induced (*sdha*, *sdhaf3*, *uqcc1* and *uqcc3*), thus further pointing to alterations of mitochondrial respiration capacity (Figure 2a). In addition, expression of known regulators of mitochondrial activity (*hebp2*, *parla*, *sirt3*) was modified upon B[a]P/ethanol co-exposure; it could be noted that *hepb2* and *parla* have been implicated in cell death (Ishihara and Mihara 2017; Szigeti et al. 2006) in agreement with the deleterious effects of B[a]P/ethanol co-exposure previously reported *in vitro* (Bucher et al. 2018b; Bucher et al. 2018a; Tête et al. 2018).

Furthermore, another key process revealed by our microarray analysis was porphyrin metabolism, notably included in the more general term of heme metabolism (as suggested by changes of expression for *tspo* and *abcg2a*) (Figure 1c). In addition, IPA identified iron homeostasis as a new process affected by B[a]P/ethanol co-exposure, which is also closely linked to heme metabolism (supplementary Table S3). Therefore, we decided to evaluate the expression of several genes associated with heme and iron metabolism (Figure 2b). Most of the changes in gene expression, found by microarray analysis, were validated by RT-qPCR (*abcb6*, *fech*, *blvra*, *blvrb*, *tfa*) (Figure 2b). In addition, co-exposure significantly altered the expression of several genes involved in heme synthesis (*alas1, alas2*), in iron transport (*slc25a37* and *slc25a28* alias mitochondrial iron transporters mitoferrin 1 and 2; *slc40a1* alias ferroportin 1), and in iron storage (*fth1a* and *fthl30*, ferritin subuntits; *tfa* for transferrin a)

(Figure 2b). Altogether, these results strongly support the idea of a perturbation in heme and iron homeostasis following B[a]P/ethanol co-exposure in our steatotic model of zebrafish larvae.

In addition, oxidative stress-related genes (markers of oxidative stress and/or genes involved in ROS/NOS production/elimination) were also investigated by RT-qPCR. Our data thus confirmed the changes observed in our microarray in the expression of catalase (*cat*) and peroxiredoxin 1 (*prdx1*); they also showed induction of *nos2a*, *prdx6*, *sod2* and *sod3b* (Figure 2c), thus suggesting the implication of oxidative stress. Finally, potential activation of AhR signaling was explored by assessing the expression of several AhR-related genes (Figure 2c). Three genes, for which expression was increased in transcriptomic analysis, were validated by RT-qPCR (*cyp1a*, *gstp1*, *nfe2le2a* alias *nrf2*). In addition, *nqo1* (NAD(P)H dehydrogenase quinone 1, an indirect target of AhR) was also found to be significantly induced by B[a]P/ethanol co-exposure as well as *ahr2*, the ortholog of human AhR (Figure 2c).

Finally, in order to evaluate the relevance of the results found in zebrafish toward human NAFLD progression upon similar co-exposure, we assessed expression of several genes related to the potential mechanisms involved (mitochondrial dysfunction, alterations of heme metabolism and iron homeostasis, and AhR signaling) in HepaRG cells, an *in vitro* human model of hepatocytes, supplemented with fatty acids (FA) in which B[a]P/ethanol co-exposure was demonstrated to induce steatosis progression toward a steatohepatitis-like state (Bucher et al. 2018b) (Figure 2d). As illustrated in Figure 2d, regarding most of the studied genes, the changes in mRNA expression observed in zebrafish larvae (as indicated by white arrows) were also reproduced in steatotic HepaRG cells co-exposed to B[a]P and ethanol, even though the amplitude of changes could be less. This is particularly observable for mRNA expression changes highly significant in zebrafish, *i.e. abcg2a*, *tspo*, *uqcc3*, *abcb6a*, *fech*, *blvra*, *slc25a37*,

slc25a28, *nqo1.* Indeed for 7 of them, significant changes were also found in HepaRG (except for ABCB6 and SLC25A28, close to significance) (Figure 2d). Therefore, these results further validated the HFD-fed zebrafish larvae as a suitable model to study human NAFLD progression, then prompting us to more thoroughly investigate the *in vivo* role of the observed alterations.

3.3. Assessment of mitochondrial dysfunction

Due to the well-recognized role of mitochondrial dysfunction in NAFLD(Begriche et al. 2013) and as it was identified in our transcriptomic analysis, we decided to evaluate mitochondrial respiration in co-exposed steatotic zebrafish larvae (Figure 3a). To this aim, we used a protocol adapted from Raftery *et al.* (2017) based on the Agilent Seahorse technology, which allows the measurement of oxygen consumption from living zebrafish larvae (Raftery et al. 2017) (described in supplementary Materials and Methods). We observed that co-exposure significantly inhibited both basal and maximal respiration without any effect on spare and non-mitochondrial respiration (Figure 3a; representative curves of OCR could be found in Figure S3). Then, in order to get further insight into mitochondrial dysfunction, we performed transmission electron microscopy (TEM) to study the ultrastructure of liver cells in co-exposed HFD zebrafish larvae (Figure 3b). Images obtained at low magnification (panel of pictures on the left) showed well-organized hepatocytes under control conditions and few biliary canaliculi. However, under B[a]P/ethanol co-exposure conditions, disorder of hepatocyte morphology was observed. Regarding more specifically the mitochondria in HFD control larvae, they appeared to represent a large part of hepatocyte surface, with a circular form and numerous cristae (central and right panels of pictures in Figure 3b) under control conditions. In contrast, after a 7-days-co-exposure to toxicants, only a few mitochondria per hepatocyte could be observed, with a smaller size and flatter form, and less observable cristae.

Therefore, these ultrastructure observations were in accordance with the decreased oxygen consumption induced by B[a]P/ ethanol co-exposure.

3.4. Involvement of AhR in *in vivo* mitochondrial dysfunction and liver damages during steatosis progression induced by B[a]P/ethanol co-exposure

AhR and/or B[a]P have already been reported to be involved in mitochondrial dysfunction in diverse *in vitro* models (Bucher et al. 2018a; Hardonnière et al. 2017; Hwang et al. 2016). Based upon the fact that our transcriptomic analysis outlined AhR signaling (see supplementary Table S3), we decided to investigate the role of this receptor in the mitochondrial dysfunction both at a transcriptomic level and at a functional level, *i.e.* mitochondrial oxygen consumption. To do so, we used the specific AhR antagonist CH223191 (1 µM) (Wang et al. 2019). To ensure that this antagonist did inhibit AhR activation in our zebrafish model, we analyzed mRNA expression of known AhR target genes after CH223191 treatment of co-exposed larvae (Figure 4a). As expected, we observed an inhibition of several B[a]P/ethanol-induced genes, *cyp1a*, *nqo1* and nfe2l2 (Figure 4a). It was not the case for *gstp1* mRNA expression; rather CH223191 alone induced its expression to a similar level as upon toxicant co-exposure, with a further increase upon co-treatment with the three molecules (Figure 4a). Thus, it probably means that the observed effect on *gstp1* expression would be a secondary response linked to its role in detoxification rather than being directly targeted by AhR. Looking at genes related to mitochondria (Figure 4b), we found that CH223191 was able to prevent co-exposure effects on *abcg2a* and partially on *sdha* (even if, for this last gene, there is no statistical difference between co-exposure conditions (BE vs CH+BE), there is no more effect of co-exposure in presence of CH223191 (CH vs CH+BE)). Regarding *tspo* and *uqcc3*, a significant induction was observed with the antagonist alone, but no further increase occurred, when larvae were co-exposed to B[a]P/ethanol (Figure 4b). Regarding heme and

iron-related genes, CH223191 reversed co-exposure effect on *fech*, *slc25a28*, *slc40a1* and *tfa* but not *blvra*, *fth1a, fthl30* and *slc25a37* (Figure 4c). Taken together, these observations suggest that AhR activation might disturb mitochondrial activity partly through a transcriptional action. In order to further test the *in vivo* role of AhR in the steatosis progression upon co-exposure, the effects of CH223191 on the expression of mRNA markers of toxicity were analyzed by RT-qPCR (Figure 4d). We found that CH223191 inhibited the increase in mRNA expression of both *casp3* and *il6,* thus suggesting reduction of cell death and inflammation, whereas it increased *prdx1* expression. As *gstp1*, this latter increase might be associated with a secondary cell response against co-exposure-induced oxidative damages. Still trying to be relevant of human NAFLD progression upon similar co-exposure, these alterations of gene expression were evaluated in AhR-knock-out HepaRG cells (Figure 4e). By this way, we found that most of the changes induced by co-exposure in the expression of genes related to mitochondria (ABCG2, UQCC3), iron homeostasis (FECH, SLC25A28, SLC40A1, TF) or, as expected, AhR activation (NFE2L2 alias NRF2 and NQO1), were prevented (Figure 4e). Finally, we investigated CH223191 effect on mitochondrial function and liver integrity (Figure 4f and g respectively). Using the Seahorse technology, we found that alterations in mitochondrial respiration induced in co-exposed HFD larvae (especially the decrease in basal respiration), were prevented by CH223191 (Figure 4f; representative curves of OCR could be found in Figure S3). We also noted that CH223191 alone could induce both maximal and non-mitochondrial respiration (Figure 4f). In addition, this AhR antagonist was able to reduce liver cell damages induced by toxicant co-exposure as shown by Hematoxylin-Eosin-Safranin (HES) staining (Figure 4g; representative pictures can be found in supplementary Figure S1). In total, these results indicate a crucial involvement of AhR in mitochondrial disruption and liver

injuries following B[a]P/ethanol co-exposure in agreement with *in vivo* progression of liver steatosis.

3.5. B[a]P/ethanol co-exposure leads to disruption of heme metabolism and to an oxidative stress involved in liver injury

As our transcriptomic data clearly pointed to heme metabolism as a possible target of B[a]P/ethanol co-exposure, alterations of this process were more thoroughly analyzed through biochemical assessment. Thus, levels of heme, hemin (the oxidized and free form of heme) and bilirubin (one of the major metabolic compounds of heme degradation) were determined in our model of HFD-fed zebrafish larvae. Co-exposure was found to increase the levels of both heme and hemin (Figure 5a and b, respectively), whereas bilirubin levels remained unchanged (Figure 5c). As increased cellular heme and hemin amounts have been reported to be toxic for cells mainly *via* oxidative stress (Kumar and Bandyopadhyay 2005), we decided to test whether B[a]P/ethanol co-exposure induced such a phenomenon under our experimental conditions, and if so, whether it was involved in the related liver damages using common antioxidants, quercetin and vitamin E (Batiha et al. 2020; Burton and Ingold 1989). Thus, lipid peroxidation was evaluated after co-exposure by fluorescent imaging using C11-bodipy$^{583/591}$ staining in liver of zebrafish larvae (Figure 5d; representative pictures can be found in supplementary Figure S4). As expected, an increase in lipid peroxidation was observed upon B[a]P/ethanol co-exposure, such an effect being prevented by quercetin (25 µM) or vitamin E (100 µM) co-treatment (Figure 5d). In order to test the involvement of oxidative stress in liver disease progression, liver damages were estimated by counting the damaged cells after histological HES staining (Figure 5e; representative pictures can be found in supplementary Figure S1). As previously reported (Bucher et al. 2018b), we found that co-exposure increased the proportion of damaged cells in liver, and quercetin as vitamin E, at

least partly, prevented this effect. These data therefore showed the involvement of oxidative stress in the pathological progression of steatosis upon B[a]P/ethanol co-exposure of HFD-fed zebrafish larvae.

3.6. Iron is a crucial player in the liver mitochondrial dysfunction and toxicity induced by B[a]P/ethanol co-exposure of HFD zebrafish larva

Our present results have highlighted the role of (i) mitochondrial dysfunction, (ii) dysregulation of heme homeostasis, and (iii) oxidative stress in co-exposure-induced *in vivo* steatosis progression. In addition, the transcriptomic analysis suggested changes in iron homeostasis, notably in mitochondria. In this context, it appeared necessary to further explore the involvement of iron homeostasis in mitochondrial dysfunction and liver toxicity under our experimental conditions. First, the level of labile iron in mitochondria (mostly represented by ferrous iron Fe^{2+} (Lv and Shang 2018)) was evaluated. To do so, alive HFD-fed zebrafish larva, co-exposed or not, were loaded with the fluorescent mitochondrial Fe^{2+}-sensitive probe, Mito-FerroGreen, followed by imaging of the liver by confocal microscopy (Figure 6a). We observed that co-exposure markedly increased the level of labile iron in mitochondria, as shown by a stronger fluorescence intensity in the liver of treated animals compared to untreated counterparts (Figure 6a, zebrafish liver is delineated by a white dot-line). In addition, quantitative analysis of liver fluorescent intensities, detected in several larvae, clearly showed the significant increase of the mitochondrial Fe^{2+} pool in liver upon B[a]P/ethanol co-exposure (Figure 6b).

In order to determine how this increase of iron might affect mitochondria and thus could lead to toxicity upon co-exposure in our zebrafish model, we decided to test the potential protective effect of the iron chelator, deferoxamine (100 µM) (Figure 6c-e). We firstly evaluated the content of liver mitochondrial Fe^{2+} using Mito-FerroGreen fluorescence

imaging. As expected, a co-treatment of larvae with deferoxamine totally prevented the increase of mitochondrial Fe^{2+} content (Figure 6c). Then, the role of iron in the toxicity was evaluated by RT-qPCR assessment of genes related to mitochondria (Figure 6d), to heme and iron homeostasis (Figure 6e), and to cellular stress and toxicity (Figure 6f). Interestingly, deferoxamine inhibited some of the changes induced by co-exposure related to mitochondria (*abcg2a*, *uqcc3*) (Figure 6d), or to iron and heme homeostasis (*fech*, *slc25a28*, *slc40a1*, *tfa*) (Figure 6e). In addition, regarding the expression of the gene markers of toxicity (*i.e. prdx1* for oxidative stress, *casp3a* for cell death and *il6* for inflammation), deferoxamine inhibited all the changes induced by co-exposure (Figure 6f). It could be noted that deferoxamine did not prevent the effects of co-exposure on the mRNA expression of *cyp1a*, *nbfe2l2* and *nqo1,* thus confirming that the protective effect of deferoxamine was linked to iron chelation rather than an inhibition of AhR signaling (Figure 6g). Finally, the role of mitochondrial iron overload in liver toxicity was confirmed by the observation of a protective effect of deferoxamine upon liver cell damages induced by B[a]P/ethanol co-exposure (Figure 6h ; representative pictures can be found in supplementary Figure S1). Taken together, these results are in favor of the involvement of an iron overload in the mitochondrial dysfunction induced by B[a]P/ethanol co-exposure, and hence related toxicity.

Finally, in order to better understand the involvement of AhR signaling in the deleterious effect of B[a]P/ethanol co-exposure on the liver, we assessed the impact of AhR inhibition on liver mitochondrial iron accumulation and oxidative stress (Figure 7 and supplementary Figure S2). Interestingly, we observed that AhR inhibition was fully protective against liver mitochondrial iron accumulation (Figure 7a) and against lipid peroxidation (Figure 7b). Therefore, these results show that AhR activation is a key event on the pathological

progression of steatosis to steatohepatitis induced by co-exposure in our zebrafish larva model.

4. Discussion

With the rise of NAFLD prevalence over the last decades, this liver disease has become a major health issue, due to its pathological complications like NASH, cirrhosis and cancer. Besides the well-known etiological factors of NAFLD (*i.e.* genetic factors, nutrition, obesity, diabetes), environmental toxicants have been put forward by an increasing number of studies; this has led to the emergence of the concept of TAFLD and TASH (Joshi-Barve et al. 2015; Wahlang et al. 2019; Wahlang et al. 2013). Recently we have found, both *in vitro* and *in vivo,* that co-exposure to B[a]P and ethanol, at doses not toxic in the absence of steatosis, could favor the NAFLD progression (Bucher et al. 2018b; Bucher et al. 2018a; Imran et al. 2018; Tête et al. 2018). In this context, several mechanisms have been identified *in vitro* including alterations of B[a]P and ethanol metabolism (Bucher et al. 2018b; Tête et al. 2018), NOS production (Tête et al. 2018), and mitochondrial dysfunction (Bucher et al. 2018a). However, the underlying mechanisms remained to be deciphered *in vivo*. To this aim, we used our recently developed model of HFD fed zebrafish larva, proven to be reliable to human models, in which B[a]P/ethanol co-exposure was involved in NAFLD steatosis progression toward a steatohepatitis-like state.

Thus, we performed a non-targeted approach by transcriptomic analysis in this model. From this, we focused on the 525 genes presenting significant changes in expression after B[a]P/ethanol co-exposure in HFD larvae. Thus, following clustering of these genes considering their expression found upon exposure to either toxicant alone or together, we performed a functional analysis based on GO enrichment (Figure 1c). Most of the annotation regarding down-regulated genes was linked to immunity. Such a result was not surprising, even in the

context of liver inflammation and NASH previously observed in our *in vivo* B[a]P/ethanol co-exposure model (Bucher et al. 2018b; Imran et al. 2018). Indeed each toxicant is known to induce immunosuppressive effects (Cella and Colonna 2015; Liamin et al. 2018; Szabo and Saha 2015). Interestingly, most of the immunosuppressive effects previously reported refer to host defense, which is coherent with the biological process term returned by functional analysis (Figure 1b; IFNg-mediated signaling pathways, neutrophil degranulation or phagocytic vesicle for example). Taken together, our results support the idea that, in the presence of NAFLD, *in vivo* exposure to toxicants might also favor infections, and doing so, potentially further aggravate liver diseases.

Concerning up-regulated genes, the functional analysis revealed a significant association with terms related to porphyrin/heme/iron metabolism, mitochondrial dysfunction, NAFLD/liver toxicity and AhR signaling (Figure 1 and supplementary Table S3). Some of these observations were in line with our recent work on the mechanisms involved in the *in vitro* impact of B[a]P/ethanol co-exposure on the progression of steatosis in the human hepatocarcinoma HepaRG cell line; indeed, we found a role for an AhR-dependent mitochondrial dysfunction (Bucher et al. 2018a). Based on this, we decided to further investigate these processes in our *in vivo* zebrafish model, with special emphasis on AhR signaling and mitochondrial iron/heme homeostasis.

Mitochondrial dysfunction is well-known to be involved in liver diseases, notably NAFLD (Grattagliano et al. 2019). From transcriptomic and RT-qPCR analysis, several alterations related to mitochondria were presently identified, with an up-regulation in the expression of several genes involved in respiratory complexe formation (*sdha, sdhaf3* in complex II, *upcc1* and *uqcc3* in complex III), and a down-regulation of *sdhc,* part of complex III (Figure 2a), thus suggesting disruption of mitochondrial respiration. Note that a similar change

422 in UQCC3 expression was also found in human HepaRG cells under these conditions (Figure
423 2d). Disruption of mitochondrial respiration in B[a]P/ethanol co-exposed HFD zebrafish larvae
424 was confirmed by the decrease in basal mitochondrial respiration (Figure 3a) prevented by
425 AhR inhibition (Figure 4f), like in co-exposed steatotic HepaRG cells (Bucher et al. 2018a). Such
426 functional alterations were related to changes in the ultrastructure of mitochondria (smaller
427 and flattened, less cristae) (Figure 3b) that might be associated with more mitochondrial
428 fission and ultimately with promotion of NAFLD, as previously reported (Li et al. 2019).
429 Considering all these results, one might then hypothesize that the decrease in mitochondria
430 respiration detected under our conditions could be associated with a decrease of the
431 respiratory chain ability to produce ATP and/or a decrease of fatty acid oxidation; both
432 potentially depending on and promoting oxidative stress in a vicious cycle (Begriche et al.
433 2019; Li et al. 2019). With respect to respiratory chain activity and related ATP production (*i.e.*
434 parameters related to oxidative phosphorylation [OXPHOS]), it is worth emphasizing that
435 B[a]P and ethanol, used alone or in combination, have already been reported to decrease
436 these parameters in steatotic human hepatocytes and other models (Begriche et al. 2019;
437 Bucher et al. 2018b; Bucher et al. 2018a; Das and Bhutia 2018; Hardonnière et al. 2016; Tête
438 et al. 2018). Such an alteration of OXPHOS is commonly associated with an increase of ROS
439 production and progression of NAFLD toward NASH particularly upon exposure to xenobiotic
440 (Wahlang et al. 2019). In line with this, a lipid peroxidation in liver was detected under our
441 experimental conditions and was found to be involved in co-exposure toxicity (Figure 5d, e).
442 Concerning AhR regulation and mitochondrial functions, it's interesting to note that
443 inhibition of AhR by the antagonist CH223191 had for some genes similar effect than co-
444 exposure (BE) (Fig 4a: *gstp1*; Fig 4b: *tspo* and *uqcc3*; Fig 4c: *fech*, *blvra*, *fth1a*, *fthl30*; Fig 4d:
445 *prdx1*). There is no clear explanation yet but such effects might rely on previously described

AhR mitochondrial pool and its consequences on mitochondrial function (Tappenden et al. 2011). In this context, compensatory mechanisms might be hypothesized.

Another altered process revealed by transcriptomic analysis was heme metabolism. Interestingly, several studies have shown that heme accumulation can favor oxidative stress and NAFLD progression, and have suggested that elevation of heme catabolism (through increase in heme oxygenase 1 (HO1), for example) could be a therapeutic perspective of NAFLD (Severson et al. 2016). In the context of steatosis progression toward a steatohepatitis-like state induced by B[a]P/ethanol co-exposure, we have found for the first time that there is an accumulation of both heme and hemin while there is no change in the heme catabolic process, as visualized by the absence of increase in bilirubin level (Figure 5), despite a significant increase in *blvra* (biliverdin reductase) gene expression (Figure 2b). Previous studies have reported that the strong AhR ligand, TCDD, could alter heme homeostasis and promote NASH in mice (Fader et al. 2017). This observation, along with our present results, would thus put heme homeostasis as a potential central hub in response to cellular chemical stress during NAFLD. As the expression of several genes of heme biosynthesis was found to be elevated in zebrafish larvae (Figure 2b) or in HepaRG cells (Figure 2d), one could suggest that heme and hemin elevations would depend on a transcriptional regulation rather than a down-regulation of the catabolic pathway. In line with this, note that no change in *hmox1a* mRNA expression was detected under our conditions (Figure 2b); furthermore, the bilirubin level remained unchanged (Figure 5c). A common consequence of heme accumulation and particularly of hemin accumulation, is an increase of oxidative stress responsible for cell death (Kumar and Bandyopadhyay 2005). Thus, the presently observed biochemical effects would fit well with the increase in lipid peroxidation and its role in hepatotoxicity (Figure 5). However, several studies have also highlighted that heme and hemin are potential inducers of cellular

antioxidant systems and could then act to protect cells against oxidative stress (Donegan et al. 2019; Luan et al. 2017). In this context, the elucidation of the precise role of heme and hemin in our *in vivo* model of pathological progression of steatosis will require further experiments.

Even if the exact role of heme homeostasis remains to be determined in our model, it is well recognized that heme metabolism is closely linked to iron homeostasis, known to cause oxidative stress through Fenton reaction, and also implicated in NAFLD (Britton et al. 2016; Corradini and Pietrangelo 2012). As a mitochondrial dysfunction was presently detected, the content of labile iron contained in mitochondria was evaluated. Despite the fact that an increased deposition of iron has previously been detected in NAFLD (Corradini and Pietrangelo 2012), to our knowledge, this is the first time that an increase (2-fold) in mitochondrial Fe^{2+} pool is observed in the context of *in vivo* pathological progression of steatosis upon exposure to toxicants (Figure 6a and b). Besides an elevation of mitochondrial iron in liver, we cannot yet exclude that iron content could also be elevated in other cell compartments, notably in ferritin complex, or in blood (bound to transferrin or hemoglobin). This elevation of mitochondrial iron was actually in agreement with the up-regulation of numerous iron-related genes like ferritin (*fth1a*, *fthl30*) and mitoferrin 1 and 2 (*slc25a37*, *slc25a28*). Interestingly, most of the gene regulations regarding iron homeostasis observed under our experimental conditions were prevented *in vivo* by CH223191 or *in vitro* in human AhR-KO HepaRG cells (Figure 4c and 4e). Thus, this strongly suggested a role for AhR in the increase in iron content. This hypothesis was confirmed by the protective effect of the AhR inhibitor CH223191 against mitochondrial iron accumulation and lipid peroxidation (Figure 7). In order to estimate the role of this mitochondrial iron accumulation in our context, we used a recognized iron chelator, namely deferoxamine (Figure 6). Not only this chelator prevented the alterations in

mitochondrial iron pool (Figure 6c) and in mRNA expression detected for most of the genes linked to heme and iron homeostasis (Figure 6e), but it also prevented the induction of gene markers of cell death (*casp3a*), inflammation (*il6*), and oxidative stress (*prdx1*) (Figure 6f); finally, it also protected from liver injuries induced by B[a]P/ethanol co-exposure (Figure 6h). It should be noted that AhR inhibition prevented, in our *in vivo* model, the decrease in mitochondrial respiration and gene transcriptomic changes related to cell death and inflammation and liver cell damages (Figure 4). Several *in vitro* and *in vivo* studies favor a role for iron in the liver alterations induced by environmental contaminants such as TCDD and polychlorinated biphenyls (PCBs) (Fader et al. 2017; Smith et al. 1995). Especially concerning B[a]P toxicity, this PAH as well as TCDD have been reported *in vivo* to modulate expression of hepcidin, to disturb heme homeostasis and to induce liver inflammation (Fader et al. 2017; Fader and Zacharewski 2017; Wang et al. 2009). Nevertheless, a clear link between xenobiotic exposure, iron overload and liver toxicity has been, so far, only demonstrated *in vivo* for TCDD, but not for B[a]P (Fader and Zacharewski 2017). Nonetheless, B[a]P was shown *in vitro* to increase iron uptake in an hepatic cell line with consecutive increase of oxidative stress and cell death (Gorria et al. 2006b). Regarding co-exposure to B[a]P and ethanol, only one study, from our team, has previously demonstrated *in vitro* that this mixture induced an iron overload responsible for an exacerbation of oxidative stress, and hence of hepatocyte death (Collin et al. 2014). Considering the mechanisms of iron accumulation, several possibilities could be proposed and will need to be further investigated in future. First, transcriptional regulation induced by co-exposure might favor iron uptake and retention, and limit iron export from liver. This hypothesis is coherent with the induction of genes such as ferritins (*fth1a*, *fthl30*) and mitoferrin (*slc25a37*, *slc25a28*) in our co-exposed HFD-fed zebrafish larvae model, and with increase of iron uptake in F258 hepatic cells following B[a]P exposure (Gorria et al.

2006b). The second possibility refers to membrane remodeling, *i.e* change in membrane fluidity and/or modulation of lipid raft signaling. Indeed, such a membrane remodeling has been involved in B[a]P-induced iron elevation and apoptosis in rat hepatic epithelial F258 cells (Gorria et al. 2006a), and in labile iron increase, lysosomal membrane permeabilization, oxidative stress and cell death induced cooperatively by B[a]P and ethanol in hepatic WIF-B9 cells (Collin et al. 2014). Regarding this latter point, it is worth noting that we previously demonstrated an implication of membrane remodeling in the pathological progression of steatosis in our model of HFD-fed zebrafish larvae upon B[a]P/ethanol co-exposure (Imran et al. 2018).

Altogether, our data strongly indicate that mitochondrial iron accumulation, dependent on AhR activation, would be largely responsible for the progression from steatosis to a steatohepatitis-like state following B[a]P/ethanol co-exposure. Iron accumulation, notably in mitochondria, is thus shown for the first time to our knowledge as a key event in toxicant-induced liver disease exacerbation in a context of NAFLD. Remarkably, these conclusions seem to be relevant of human heath as iron deposition in human liver has been correlated with oxidative stress and progression toward steatohepatitis or fibrosis (Britton et al. 2016). However, the role for xenobiotic exposure, particularly in mixture, in human liver iron overload and NAFLD is still not elucidated and need to be explored. In this context, one interesting concept should be investigated deeper : the ferroptosis. Ferroptosis is a recently described specific type of non-apoptotic cell death dependant on iron and lipid peroxidation (Cao and Dixon 2016; Mou et al. 2019; Qi et al. 2020; Tsurusaki et al. 2019). Thus, ferroptosis is known to be suppressed by iron chelators as deferoxamine and with antioxidants (Mou et al. 2019; Tsurusaki et al. 2019) which is very coherent with results observed in our zebrafish model. In addition, this type of cell death has been also associated with NASH progression (Qi

et al. 2020; Tsurusaki et al. 2019). Under our experimental conditions, it would thus be interesting to test such an involvement of ferroptosis notably by testing the effects of a specific inhibitor, like ferrostatin-1 (Cao and Dixon 2016; Skouta et al. 2014).

Conclusions

On the whole, this study, using a model of HFD-fed steatotic zebrafish larva, has shed new light on the mechanisms involved in the *in vivo* transition of liver steatosis toward steatohepatitis-like state induced by B[a]P/ethanol co-exposure. Indeed, this co-exposure activates AhR, then leading to transcriptomic alterations of heme and iron homeostasis, and also of mitochondrial functions. The consequences of such alterations were notably an elevation of heme and hemin content in zebrafish larvae, probably dependent on an increase in heme synthesis, since no change in bilirubin could be observed. The role of heme and hemin are still speculative but they most likely play a role in NAFLD progression through oxidative stress. Looking at mitochondrial disruptions, the main changes impacted morphology (smaller and flattened mitochondria), mitochondrial respiration, and labile iron (Fe^{2+}) content. We proposed that iron overload in mitochondria, possibly depending on AhR activation and likely acting *via* oxidative stress, would represent a key event in the steatosis progression induced by B[a]P/ethanol co-exposure of HFD zebrafish larvae as iron chelation has been found to be largely protective towards cell death and inflammation.

Acknowledgements

We first wish to thank INRA-LPGP (Institut National de la Recherche Agronomique, Laboratoire de Physiologie et Génomique des Poissons, Rennes, France) for providing zebrafish eggs. We

566 are also very grateful to MRiC and H2P2 platforms (UMS BIOSIT, Rennes, France), notably
567 Stéphanie Dutertre (MRic) for confocal microscopic imagery, Alain Fautrel and Pascal Belaud
568 (H2P2) for their help on histological staining, and finally Agnes Burel (MRiC) for her expertise
569 on electron microscopy. We also wish to thank Dr Olivier Loréal (UMR 1241, Inserm, Rennes)
570 for the fruitful discussion regarding iron homeostasis. Muhammad Imran was the recipient of
571 a fellowship from the Higher Education Commission, Pakistan. Simon Bucher was recipient of
572 fellowships from the Région Bretagne (ARED) and from the Agence Nationale de la Recherche
573 (ANR). We also wish to thank ANR and the Institut Thématique Multi-Organisme Cancer (ITMO
574 Cancer) d'Aviesan for financial supports to our work (STEATOX project, “ANR-13-CESA-0009”
575 and METAhCOL project, n°17CE040_00).

576

577 Funding: This work was supported by the Agence Nationale de la Recherche (ANR) and the
578 Institut Thématique Multi-Organisme Cancer (ITMO Cancer) d'Aviesan (STEATOX project,
579 “ANR-13-CESA-0009” and METAhCOL project, n°17CE040_00).

580

581 Author contribution: Conception and design of the study (NP, MI, DLG, OS); Acquisition of data
582 (MI, FC, BE, HLM, AD, MB, SB, AL); Analysis and interpretation of data (MI, NP, DLG, FC, LS,
583 LH); Drafting the article or revising it critically for important intellectual content (MI, NP, DLG,
584 OS, LS, BF, LH).

585 Data Availability: All transcriptomic data are available in our supplemental files.

586 **Declarations**

Ethics approval: All animal experiments were in agreement with the European Union regulations concerning the use and protection of experimental animals (Directive 2010/63/EU). All protocols were approved by local ethic committee CREEA (Comité Rennais d'Ethique en matière d'Expérimentation Animale)

Consent for publication: All authors approve of this submission for publication.

Competing interests: The authors declare no competing interests.

References

Batiha GE-S, Beshbishy AM, Ikram M, Mulla ZS, El-Hack MEA, Taha AE, et al. The Pharmacological Activity, Biochemical Properties, and Pharmacokinetics of the Major Natural Polyphenolic Flavonoid: Quercetin. Foods. 2020 Mar 23;9(3):374.

Begriche K, Massart J, Fromenty B. Mitochondrial Dysfunction Induced by Xenobiotics: Involvement in Steatosis and Steatohepatitis. Mitochondria Obes. Type 2 Diabetes [Internet]. Elsevier; 2019 [cited 2019 Aug 23]. p. 347–64. Available from: https://linkinghub.elsevier.com/retrieve/pii/B9780128117521000158

Begriche K, Massart J, Robin M-A, Bonnet F, Fromenty B. Mitochondrial adaptations and dysfunctions in nonalcoholic fatty liver disease. Hepatol. Baltim. Md. 2013 Oct;58(4):1497–507.

Britton LJ, Subramaniam VN, Crawford DH. Iron and non-alcoholic fatty liver disease. World J. Gastroenterol. 2016 Sep 28;22(36):8112–22.

Bucher S, Le Guillou D, Allard J, Pinon G, Begriche K, Tête A, et al. Possible Involvement of Mitochondrial Dysfunction and Oxidative Stress in a Cellular Model of NAFLD Progression Induced by Benzo[a]pyrene/Ethanol CoExposure. Oxid. Med. Cell. Longev. 2018a;2018:4396403.

Bucher S, Tête A, Podechard N, Liamin M, Le Guillou D, Chevanne M, et al. Co-exposure to benzo[a]pyrene and ethanol induces a pathological progression of liver steatosis in vitro and in vivo. Sci. Rep. 2018b Apr 13;8(1):5963.

Burton GW, Ingold KU. Vitamin E as an in Vitro and in Vivo Antioxidant. Ann. N. Y. Acad. Sci. 1989 Dec;570(1 Vitamin E):7–22.

Cao JY, Dixon SJ. Mechanisms of ferroptosis. Cell. Mol. Life Sci. CMLS. 2016 Jun;73(11–12):2195–209.

Cella M, Colonna M. Aryl hydrocarbon receptor: Linking environment to immunity. Semin. Immunol. 2015 Sep;27(5):310–4.

Chu J, Sadler KC. New school in liver development: lessons from zebrafish. Hepatol. Baltim. Md. 2009 Nov;50(5):1656–63.

Collin A, Hardonnière K, Chevanne M, Vuillemin J, Podechard N, Burel A, et al. Cooperative interaction of benzo[a]pyrene and ethanol on plasma membrane remodeling is responsible for enhanced oxidative stress and cell death in primary rat hepatocytes. Free Radic. Biol. Med. 2014 Jul;72:11–22.

Corradini E, Pietrangelo A. Iron and steatohepatitis. J. Gastroenterol. Hepatol. 2012 Mar;27 Suppl 2:42–6.

Das DN, Bhutia SK. Inevitable dietary exposure of Benzo[a]pyrene: carcinogenic risk assessment an emerging issues and concerns. Curr. Opin. Food Sci. 2018 Dec;24:16–25.

Donegan RK, Moore CM, Hanna DA, Reddi AR. Handling heme: The mechanisms underlying the movement of heme within and between cells. Free Radic. Biol. Med. 2019 Mar;133:88–100.

Driessen M, Kienhuis AS, Pennings JLA, Pronk TE, van de Brandhof E-J, Roodbergen M, et al. Exploring the zebrafish embryo as an alternative model for the evaluation of liver toxicity by histopathology and expression profiling. Arch. Toxicol. 2013 May;87(5):807–23.

Driessen M, Kienhuis AS, Vitins AP, Pennings JLA, Pronk TE, van den Brandhof E-J, et al. Gene expression markers in the zebrafish embryo reflect a hepatotoxic response in animal models and humans. Toxicol. Lett. 2014 Oct 1;230(1):48–56.

Fader KA, Nault R, Kirby MP, Markous G, Matthews J, Zacharewski TR. Convergence of hepcidin deficiency, systemic iron overloading, heme accumulation, and REV-ERBα/β activation in aryl hydrocarbon receptor-elicited hepatotoxicity. Toxicol. Appl. Pharmacol. 2017 Apr;321:1–17.

Fader KA, Zacharewski TR. Beyond the Aryl Hydrocarbon Receptor: Pathway Interactions in the Hepatotoxicity of 2,3,7,8-Tetrachlorodibenzo-p-dioxin and Related Compounds. Curr. Opin. Toxicol. 2017 Feb;2:36–41.

Fazel Y, Koenig AB, Sayiner M, Goodman ZD, Younossi ZM. Epidemiology and natural history of non-alcoholic fatty liver disease. Metabolism. 2016 Aug;65(8):1017–25.

Goessling W, Sadler KC. Zebrafish: An Important Tool for Liver Disease Research. Gastroenterology. 2015 Nov;149(6):1361–77.

Goldstone JV, McArthur AG, Kubota A, Zanette J, Parente T, Jönsson ME, et al. Identification and developmental expression of the full complement of Cytochrome P450 genes in Zebrafish. BMC Genomics. 2010;11:643.

Goodale BC, La Du JK, Bisson WH, Janszen DB, Waters KM, Tanguay RL. AHR2 mutant reveals functional diversity of aryl hydrocarbon receptors in zebrafish. PloS One. 2012;7(1):e29346.

Gorria M, Huc L, Sergent O, Rebillard A, Gaboriau F, Dimanche-Boitrel M-T, et al. Protective effect of monosialoganglioside GM1 against chemically induced apoptosis through targeting of mitochondrial function and iron transport. Biochem. Pharmacol. 2006a Nov;72(10):1343–53.

Gorria M, Tekpli X, Sergent O, Huc L, Gaboriau F, Rissel M, et al. Membrane fluidity changes are associated with benzo[a]pyrene-induced apoptosis in F258 cells: protection by exogenous cholesterol. Ann. N. Y. Acad. Sci. 2006b Dec;1090:108–12.

Grattagliano I, Montezinho LP, Oliveira PJ, Frühbeck G, Gómez-Ambrosi J, Montecucco F, et al. Targeting mitochondria to oppose the progression of nonalcoholic fatty liver disease. Biochem. Pharmacol. 2019 Feb;160:34–45.

Hardonnière K, Fernier M, Gallais I, Mograbi B, Podechard N, Le Ferrec E, et al. Role for the ATPase inhibitory factor 1 in the environmental carcinogen-induced Warburg phenotype. Sci. Rep. 2017 15;7(1):195.

Hardonnière K, Saunier E, Lemarié A, Fernier M, Gallais I, Héliès-Toussaint C, et al. The environmental carcinogen benzo[a]pyrene induces a Warburg-like metabolic reprogramming dependent on NHE1 and associated with cell survival. Sci. Rep. 2016 04;6:30776.

Hwang HJ, Dornbos P, Steidemann M, Dunivin TK, Rizzo M, LaPres JJ. Mitochondrial-targeted aryl hydrocarbon receptor and the impact of 2,3,7,8-tetrachlorodibenzo-p-dioxin on cellular respiration and the mitochondrial proteome. Toxicol. Appl. Pharmacol. 2016 01;304:121–32.

Imran M, Sergent O, Tête A, Gallais I, Chevanne M, Lagadic-Gossmann D, et al. Membrane Remodeling as a Key Player of the Hepatotoxicity Induced by Co-Exposure to Benzo[a]pyrene and Ethanol of Obese Zebrafish Larvae. Biomolecules. 2018 14;8(2).

International Agency for Research on Cancer (IARC). Chemical Agents and Related Occupations. [Internet]. Place of publication not identified: publisher not identified; 2012 [cited 2019 Sep 3]. Available from: http://VH7QX3XE2P.search.serialssolutions.com/?V=1.0&L=VH7QX3XE2P&S=AC_T_B&C=Chemical%20Agents%20and%20Related%20Occupations&T=marc&tab=BOOKS

Ishihara N, Mihara K. PARL paves the way to apoptosis. Nat. Cell Biol. 2017 31;19(4):263–5.

Joshi-Barve S, Kirpich I, Cave MC, Marsano LS, McClain CJ. Alcoholic, Nonalcoholic, and Toxicant-Associated Steatohepatitis: Mechanistic Similarities and Differences. Cell. Mol. Gastroenterol. Hepatol. 2015 Jul;1(4):356–67.

Kumar S, Bandyopadhyay U. Free heme toxicity and its detoxification systems in human. Toxicol. Lett. 2005 Jul 4;157(3):175–88.

Li Z, Li Y, Zhang H-X, Guo J-R, Lam CWK, Wang C-Y, et al. Mitochondria-Mediated Pathogenesis and Therapeutics for Non-Alcoholic Fatty Liver Disease. Mol. Nutr. Food Res. 2019 Jun 14;e1900043.

Liamin M, Le Mentec H, Evrard B, Huc L, Chalmel F, Boutet-Robinet E, et al. Genome-Wide Transcriptional and Functional Analysis of Human T Lymphocytes Treated with Benzo[α]pyrene. Int. J. Mol. Sci. 2018 Nov 17;19(11).

Luan Y, Zhang F, Cheng Y, Liu J, Huang R, Yan M, et al. Hemin Improves Insulin Sensitivity and Lipid Metabolism in Cultured Hepatocytes and Mice Fed a High-Fat Diet. Nutrients. 2017 Jul 26;9(8):805.

Lv H, Shang P. The significance, trafficking and determination of labile iron in cytosol, mitochondria and lysosomes. Met. Integr. Biometal Sci. 2018 18;10(7):899–916.

Mou Y, Wang J, Wu J, He D, Zhang C, Duan C, et al. Ferroptosis, a new form of cell death: opportunities and challenges in cancer. J. Hematol. Oncol.J Hematol Oncol. 2019 Mar 29;12(1):34.

693 Qi J, Kim J-W, Zhou Z, Lim C-W, Kim B. Ferroptosis Affects the Progression of Nonalcoholic
694 Steatohepatitis via the Modulation of Lipid Peroxidation-Mediated Cell Death in Mice. Am. J. Pathol.
695 2020 Jan;190(1):68–81.

696 Raftery TD, Jayasundara N, Di Giulio RT. A bioenergetics assay for studying the effects of
697 environmental stressors on mitochondrial function in vivo in zebrafish larvae. Comp. Biochem.
698 Physiol. Part C Toxicol. Pharmacol. 2017 Feb;192:23–32.

699 Schlegel A. Studying non-alcoholic fatty liver disease with zebrafish: a confluence of optics, genetics,
700 and physiology. Cell. Mol. Life Sci. CMLS. 2012 Jun 8;

701 Severson TJ, Besur S, Bonkovsky HL. Genetic factors that affect nonalcoholic fatty liver disease: A
702 systematic clinical review. World J. Gastroenterol. 2016;22(29):6742.

703 Skouta R, Dixon SJ, Wang J, Dunn DE, Orman M, Shimada K, et al. Ferrostatins inhibit oxidative lipid
704 damage and cell death in diverse disease models. J. Am. Chem. Soc. 2014 Mar 26;136(12):4551–6.

705 Smith AG, Carthew P, Clothier B, Constantin D, Francis JE, Madra S. Synergy of iron in the toxicity and
706 carcinogenicity of polychlorinated biphenyls (PCBs) and related chemicals. Toxicol. Lett. 1995
707 Dec;82–83:945–50.

708 Szabo G, Saha B. Alcohol's Effect on Host Defense. Alcohol Res. Curr. Rev. 2015;37(2):159–70.

709 Szigeti A, Bellyei S, Gasz B, Boronkai A, Hocsak E, Minik O, et al. Induction of necrotic cell death and
710 mitochondrial permeabilization by heme binding protein 2/SOUL. FEBS Lett. 2006 Nov
711 27;580(27):6447–54.

712 Tappenden DM, Lynn SG, Crawford RB, Lee K, Vengellur A, Kaminski NE, et al. The aryl hydrocarbon
713 receptor interacts with ATP5α1, a subunit of the ATP synthase complex, and modulates
714 mitochondrial function. Toxicol. Appl. Pharmacol. 2011 Aug 1;254(3):299–310.

715 Tekpli X, Rissel M, Huc L, Catheline D, Sergent O, Rioux V, et al. Membrane remodeling, an early
716 event in benzo[a]pyrene-induced apoptosis. Toxicol. Appl. Pharmacol. 2010 Feb 15;243(1):68–76.

717 Tête A, Gallais I, Imran M, Chevanne M, Liamin M, Sparfel L, et al. Mechanisms involved in the death
718 of steatotic WIF-B9 hepatocytes co-exposed to benzo[a]pyrene and ethanol: a possible key role for
719 xenobiotic metabolism and nitric oxide. Free Radic. Biol. Med. 2018;129:323–37.

720 Tsurusaki S, Tsuchiya Y, Koumura T, Nakasone M, Sakamoto T, Matsuoka M, et al. Hepatic ferroptosis
721 plays an important role as the trigger for initiating inflammation in nonalcoholic steatohepatitis. Cell
722 Death Dis. 2019 Jun 18;10(6):449.

723 Uno S, Nebert DW, Makishima M. Cytochrome P450 1A1 (CYP1A1) protects against nonalcoholic fatty
724 liver disease caused by Western diet containing benzo[a]pyrene in mice. Food Chem. Toxicol. Int. J.
725 Publ. Br. Ind. Biol. Res. Assoc. 2018 Mar;113:73–82.

726 Wahlang B, Beier JI, Clair HB, Bellis-Jones HJ, Falkner KC, McClain CJ, et al. Toxicant-associated
727 steatohepatitis. Toxicol. Pathol. 2013 Feb;41(2):343–60.

728 Wahlang B, Jin J, Beier JI, Hardesty JE, Daly EF, Schnegelberger RD, et al. Mechanisms of
729 Environmental Contributions to Fatty Liver Disease. Curr. Environ. Health Rep. 2019 Sep;6(3):80–94.

730 Wang E, Liu X, Tu W, Do DC, Yu H, Yang L, et al. Benzo(a)pyrene facilitates dermatophagoides group 1
731 (Der f 1)-induced epithelial cytokine release through aryl hydrocarbon receptor in asthma. Allergy.
732 2019 Sep;74(9):1675–90.

733 Wang K-J, Bo J, Yang M, Hong H-S, Wang X-H, Chen F-Y, et al. Hepcidin gene expression induced in
734 the developmental stages of fish upon exposure to Benzo[a]pyrene (BaP). Mar. Environ. Res. 2009
735 Apr;67(3):159–65.

736 Younossi ZM. Non-alcoholic fatty liver disease - A global public health perspective. J. Hepatol. 2019
737 Mar;70(3):531–44.

738
739

Supplementary material captions:

- **Supplementary file S1:** Details for all Materials and methods.
- **Supplementary Figure S1:** Illustrations of histological sections of zebrafish larvae to evaluate liver damages upon B[a]P/ethanol co-exposure of steatotic zebrafish larva with or without co-treatment with protective agents.
- **Supplementary Figure S2:** Illustrations of fluorescent staining of zebrafish larvae to evaluate liver mitochondrial iron accumulation and lipid peroxidation upon B[a]P/ethanol co-exposure of steatotic zebrafish larva with or without co-treatment with AhR antagonist, CH223191.
- **Supplementary Figure S3:** Effect of B[a]P/ethanol co-exposure on oxygen consumption rale in zebrafish larva and impact of the AhR antagonist, CH223191 (OCR curves).
- **Supplementary Figure S4:** Illustrations of fluorescent staining of zebrafish larvae to evaluate lipid peroxidation upon B[a]P/ethanol co-exposure of steatotic zebrafish larvae with or without co-treatment with an antioxidant, quercetin or vitamin E.
- **Supplementary Table S1:** Excel file containing fold change data of the 525 DEGs.
- **Supplementary Table S2:** Excel file containing the table of conversion of the 525 zebrafish DEGs into 259 human homologs with associated retained fold change.
- **Supplementary Table S3:** Excel file containing the table of several terms resulted from the Ingenuity Pathways Analysis (IPA) of the 259 human homologs of DEGs.
- **Supplementary Table S4:** Excel file containing tables of full results from the Ingenuity Pathways Analysis (IPA) of the 259 human homologs of DEGs.
- **Supplementary Table S5:** Excel file containing tables of sequences of the tested primers used in RT-qPCR.
- **Supplementary Table S6:** Excel file containing all compiled data and sample size information.

Figure legends:

Figure 1 Transcriptomic analyses reveal major-disrupted targets such as heme homeostasis and mitochondria in B[a]P/ethanol co-exposed zebrafish larvae. Transcriptomic analyses using GeneChip™ Zebrafish gene 1.0 ST array were performed on mRNA samples from 12 dpf HFD-fed zebrafish larvae exposed to 25 nM B[a]P and/or 43 mM ethanol during 7 days (n=5). (**a**) A flow chart outlines transcriptomic approach and statistical analysis for gene selection and clustering. (**b**) A heat-map summarizes changes of expression of the 525 B[a]P/ethanol (BE)-modulated transcripts and their clustering depending on each condition. (**c**) Table indicate main results of gene ontology enrichment analysis using AMEN tool on GO and KEGG annotations. For each set of genes (up- and down-regulated ones in intense red and blue color, respectively; patterns [P1 to P8] in light red or blue color), significant enriched terms are given with an enrichment ratio indicating the number of annotated genes recovered out of the number of genes expected for this annotation

Figure 2 Validation of zebrafish transcriptomic screening and relevance in human HepaRG cells. (**a**, **b**, **c**) Zebrafish larvae were fed with HFD from 4 dpf and then treated with control vehicle (C) or exposed to 25nM B[a]P and 43 mM ethanol (BE) for seven days (from 5 to 12 dpf). mRNA samples were collected from pools of 10 to 20 larvae, and mRNA expression was evaluated by quantitative reverse transcription polymerase chain reaction (RT-qPCR) for different groups of function-related genes, *i.e.* mitochondria-related genes (**a**) (n≥10), heme & iron-related genes (**b**) (n≥5), oxidative stress & AhR signaling-related genes (**c**) (n≥7). (**d**) HepaRG cells were supplemented with fatty acids for 2 days (150 µM stearic acid and 150 µM oleic acid) and co-treated (BE) or not (C) with B[a]P (2.5 µM) and ethanol (25mM) for 2 weeks (see reference (Bucher et al. 2018b) for further details) (n≥3). mRNA expression was evaluated by RT-qPCR for different groups of function-related genes. Data are expressed relative to mRNA levels found in control condition (C), set at 0 (log 2 change). Values are the mean ± SEM. *, **, *** statistically different from HFD control with respectively $p<0.05$; $p<0.01$ and $p<0.001$. Trends of change in gene expression found in zebrafish either in microarray (**a**, **b**, **c**) or by RT-qPCR (**d**) are indicated by white arrows when consistent with microarray or RT-qPCR observations or in grey arrows when not (by an up arrow for up-regulated genes and down arrow for down regulated genes)

Figure 3 Evaluation of mitochondrial alterations induced by B[a]P/ethanol co-exposure in liver of steatotic zebrafish larva. Zebrafish larvae were fed with HFD from 4 dpf and then treated at 5 dpf with control vehicle (C) or exposed to B[a]P and ethanol (BE) (1 µM B[a]P + 173 mM ethanol for 1 day in (**a**), or 25 nM B[a]P + 43 mM ethanol for 7 days in (**b**)). (**a**) Measurement on Seahorse XFe24 Analyzer of mitochondrial oxygen consumption in zebrafish larva. Values are the mean of oxygen consumption rate (OCR, in pmol of O_2/min) ± SEM measured from at least 7 larvae per condition. *, **, *** statistically different from HFD control with respectively $p<0.05$; $p<0.01$ and $p<0.001$. (**b**) Zebrafish liver section imaging by transmission electronic microscopy. Left panels present a large view of liver section (magnification 5000x) whereas the middle ones show images of hepatocyte (magnification 8000x), with higher magnification in right panels to better evaluate mitochondria morphologies (digital magnification of previous images 3x). Images are representative of 3 larvae per condition (BC, biliary canaliculi; N, nucleus; M, mitochondria; in right panel, examples of mitochondrial cristae are indicated by a red arrow head)

Figure 4 Involvement of AhR activation in mitochondrial dysfunction and liver toxicity induced by B[a]P/ethanol co-exposure. Zebrafish larvae were fed with HFD from 4 dpf and then treated at 5 dpf with control vehicle (C) or exposed to B[a]P and ethanol (BE) (25 nM B[a]P + 43 mM ethanol for 7 days in (**a-d, g**) or 1 µM B[a]P + 173 mM ethanol for 1 day in (**f**). For these experiments, some larvae were also co-treated with 1 µM CH223191 (CH), a specific AhR antagonist. In (**e**), HepaRG cells wild-type (WT) or knock-out for AhR (KO) (see reference (Bucher et al. 2018a) for details) were supplemented with fatty acids during 2 days (150 µM stearic acid and 150 µM oleic acid) and co-treated (BE) or not (C) with B[a]P (2.5 µM) and ethanol (25 mM) for 2 weeks. mRNA expression was evaluated by quantitative reverse transcription polymerase chain reaction (RT-qPCR) for different groups of function-related genes in zebrafish, i.e. AhR signaling-related genes (**a**) (n≥4), mitochondria-related genes (**b**) (n≥4), heme & iron-related genes (**c**) (n≥4), oxidative stress, cell-death and inflammation genes (**d**) (n≥4) and in HepaRG cells (**e**) (n≥3). Data are expressed relative to mRNA levels found in HFD untreated control larvae (C) (**a** to **d**) or in HepaRG WT control cells (**e**), set at 0 (log 2 change). RT-qPCR values are the mean ± SEM. (**f**) Measurement on Seahorse XFe24 Analyzer of mitochondrial oxygen consumption in zebrafish larva. Values are the mean of oxygen consumption rate (OCR, in pmol of O_2/min) ± SEM measured from at least 5 larvae per condition. (**g**) Counting of liver damaged cells was performed on histological sections of zebrafish stained by HES from at least 3 larvae per condition. Values are the mean ± SEM. * indicates a statistically significant effect of BE co-exposure *vs* control counterpart in presence or not of CH (BE vs C and CH+BE vs CH) with p<0.05 (**a** to **g**); § indicates a statistically significant effect of CH223191 inhibitor *vs* counterpart without CH (CH vs C and CH+BE vs BE) with p<0.05 (**a-d**, **f**, **g**); # indicates a statistically significant interaction between co-exposure and inhibitor (**a-d**, **f**, **g**) or between co-exposure and AhR knock-out (**e**) with p<0.05

Figure 5 Disruption of heme metabolism and involvement of oxidative stress in liver injury induced by B[a]P/ethanol co-exposure. Zebrafish larvae were fed with HFD from 4 dpf and then treated with control vehicle (C) or exposed to 25 nM B[a]P and 43 mM ethanol (BE) for 7 days (from 5 to 12 dpf). Some larvae were also co-treated with 25 µM quercetin (Que) or 100 µM vitamin E (Vit E). Levels of heme (**a**) (n≥18), hemin (**b**) (n≥7) and bilirubin (**c**) (n≥11) were evaluated from homogenates of pools of whole larva. (**d**) Lipid peroxidation, marker of oxidative stress, was assessed in zebrafish larvae by quantification of fluorescence intensities in liver following staining of larvae with C11-Bodipy $^{581/591}$ (BC11) (n≥6). (**e**) Counting of liver damaged cells was performed on histological sections of zebrafish stained by HES from at least 3 larvae per condition. Values are the mean ± SEM. *, **, *** indicate a statistically significant effect of BE co-exposure *vs* control counterpart in presence or not of antioxidant (BE vs C; Que+BE vs Que; Vit E+BE vs Vit E) with p<0.05, p<0.01 and p<0.001 respectively; § indicates a statistically significant effect of quercetin or vitamin E *vs* counterpart without antioxidant (Que vs C; Que+BE vs BE; Vit E vs C; Vit E+BE vs BE) with p<0.05 (**d**, **e**); # indicates a statistically significant interaction between co-exposure and antioxidant (**d**, **e**) with p<0.05

Figure 6 Involvement of iron accumulation in liver mitochondrial dysfunction and toxicity induced by B[a]P/ethanol co-exposure of steatotic zebrafish larva. Zebrafish larvae were fed with HFD from 4 dpf and then treated with control vehicle (C) or exposed to 25 nM B[a]P and 43 mM ethanol (BE) for 7 days (from 5 to 12 dpf). Some larvae were also co-treated with an iron chelator, 100 µM deferoxamine (Def). (**a**) Imaging of free iron (Fe^{2+}) in the liver of

zebrafish larvae was done by confocal microscopy after staining with Mito-FerroGreen probe. Merge of transmitted light and green fluorescent imaging are given in upper panels whereas bottom panels present enlargement of liver only in green fluorescent channel (magnification x200; dotted line outline liver). For each picture presented in bottom panels, the mean fluorescent intensity (MFI) determined is indicated. (**b**) Relative mitochondrial iron content was assessed by quantification of green fluorescent intensities, found in liver of zebrafish using previous confocal images (n≥9). (**c**) Relative mitochondrial iron content was assessed by quantification of Mito-FerroGreen fluorescence intensities, detected in the liver of zebrafish using confocal images in the presence or not of Def (n≥9). mRNA expression was evaluated by quantitative reverse transcription polymerase chain reaction (RT-qPCR) for different groups of function-related genes in zebrafish, *i.e.* mitochondria-related genes (**d**) (n≥3), heme & iron-related genes (**e**) (n≥3), oxidative stress, cell-death and inflammation genes (**f**) (n≥3), and AhR signaling-related genes (**g**) (n≥4) in the presence or not of Def. (**h**) Liver damaged cells counting was performed on histological sections of zebrafish stained by HES from at least 4 larvae per condition in the presence or not of Def. Values are the mean ± SEM. *, **, *** indicate a statistically significant effect of BE co-exposure *vs* control counterpart in presence or not of Def (BE vs C and Def+BE vs Def) with $p<0.05$, $p<0.01$ and $p<0.001$ respectively; § indicates a statistically significant effect of deferoxamine *vs* counterpart without Def (Def vs C and Def+BE vs BE) with $p<0.05$ (**b** to **h**); # indicates a statistically significant interaction between co-exposure and deferoxamine treatment (**b** to **h**) with $p<0.05$

Figure 7: Involvement of AhR in liver mitochondrial iron accumulation and lipid peroxidation induced by B[a]P/ethanol co-exposure of steatotic zebrafish larva. Zebrafish larvae were fed with HFD from 4 dpf and then treated with control vehicle (C) or exposed to 25 nM B[a]P and 43 mM ethanol (BE) for 7 days (from 5 to 12 dpf). Some larvae were also co-treated with a protective agent: 1 µM CH223191 (CH). (**a**) The relative mitochondrial iron content was assessed by quantification of green fluorescence intensities in the liver using confocal images. (**b**) Lipid peroxidation, a marker of oxidative stress, was assessed in zebrafish larvae by quantification of fluorescence intensities in the liver following staining with C11-Bodipy $^{581/591}$ (BC11). Values are the mean ± SEM (n≥7). *, **, *** indicate a statistically significant effect of BE co-exposure *vs* control counterpart in presence or not of CH (BE vs C and CH+BE vs CH) with $p<0.05$, $p<0.01$ and $p<0.001$ respectively; § indicates a statistically significant effect of CH *vs* counterpart without CH (CH vs C; CH+BE vs BE) with $p<0.05$; # indicates a statistically significant interaction between co-exposure and CH treatment with $p<0.05$.

a

- **5 Pools of mRNA**
(each from 25 whole HFD-fed larva per condition)
- GeneChip™ Zebrafish Gene 1.0 ST array

Dectectable transcripts
Signals ≥ overall median (6.42)
Differential expression
Fold-change BE vs C ≥ ±1.3

Statistical test
p-value (FDR) ≤ 0.001

525 BE-modulated transcripts
315 Up-regulated
210 Down-regulated

Clustering

8 expression patterns
4 Up (P1-P4)
4 Down (P5-P8)

b

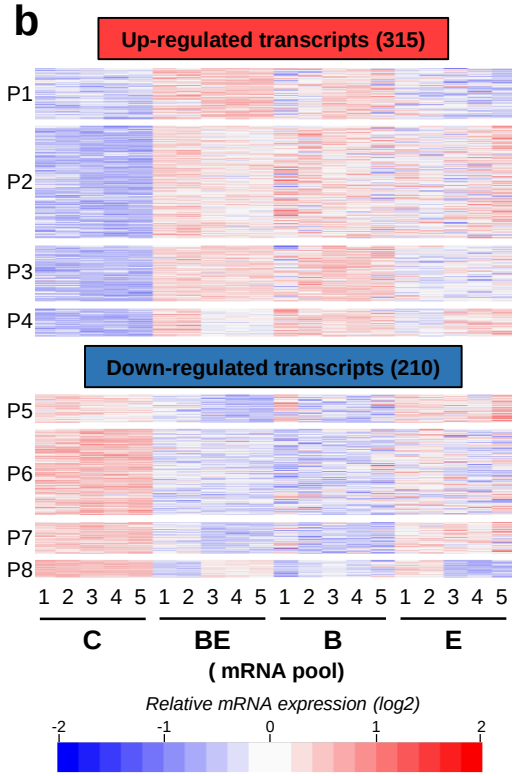

c

	Significantly enriched GO & KEGG terms (p<0.05)	Up-Regulated transcripts					Down-Regulated transcripts				
		All	P1	P2	P3	P4	All	P5	P6	P7	P8
Biological process	**porphyrin-containing compound catabolic process (GO:0006787)**	5/0		2/0	2/0	1/0					
	protein repair (GO:0030091)	3/0		2/0		1/0					
	cellular reponse to toxic substance (GO:0097237)	19/3	2/1	11/1	3/1	3/0			3/1		
	glutathione transport (GO:0034635)	4/0		3/0	1/0						
	removal of superoxide radicals (GO:0019430)	3/0		3/0							
	IFNg-mediated signaling pathway (GO:0060333)						8/0		3/0	5/0	
	neutrophil degranulation (GO:0043312)						14/3		9/2	4/1	
	antigen processing and presentation of exogenous peptide antigen (GO:0002478)						9/1		5/1	4/0	
	positive regulation of actin filament polymerization (GO:0030838)		1/0				6/1		6/0		
	cellular response to chemical stimulus (GO:0070887)	56/39	14/8	27/18			51/23		29/13	15/4	
	positive regulation of interleukin-12 production (GO:0032735)						3/0			3/0	
Cellular component	**mitochondrial membrane (GO:0031966)**	31/11	8/2	12/5	8/3	3/1					
	phagocytic vesicle membrane (GO:0030670)						6/1		4/0	2/0	
Molecular function	oxidoreductase activity… (GO0016672)	3/0	1/0	1/0		1/0					
	monooxygenase activity (GO:0004497)	9/2	3/0	3/1	2/0	1/0	3/1		2/1	1/0	
KEGG	**Porphyrin and chlorophyll metabolism (KEGG:00860)**	8/1	1/0	3/0	3/0	1/0					

Figure 1

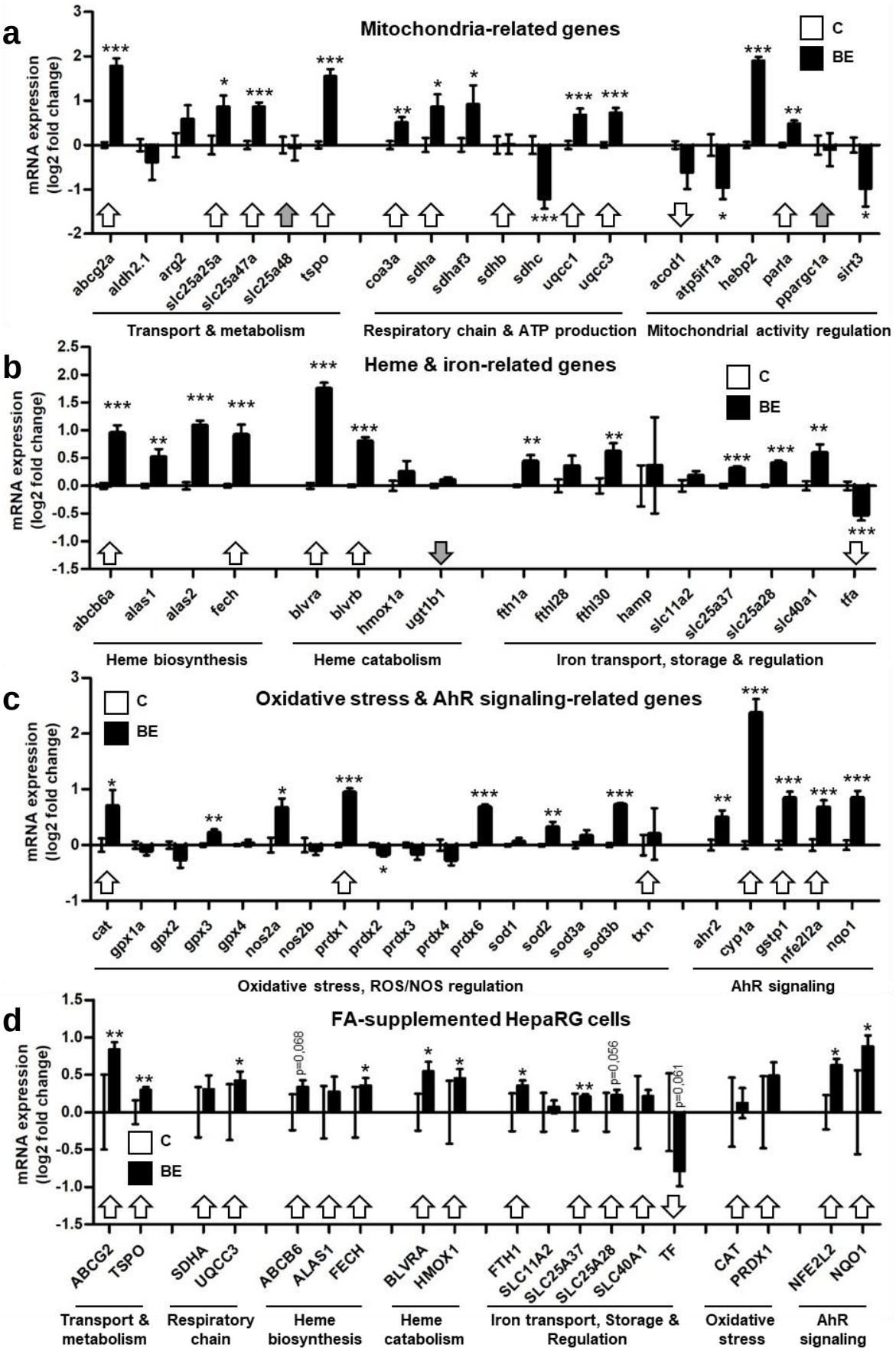
a
Mitochondria-related genes
C
BE
mRNA expression (log2 fold change)
abcg2a
aldh2.1
arg2
slc25a25a
slc25a47a
slc25a48
tspo
coa3a
sdha
sdhaf3
sdhb
sdhc
uqcc1
uqcc3
acod1
atp5if1a
hebp2
parla
ppargc1a
sirt3
Transport & metabolism
Respiratory chain & ATP production
Mitochondrial activity regulation
b
Heme & iron-related genes
C
BE
mRNA expression (log2 fold change)
abcb6a
alas1
alas2
fech
blvra
blvrb
hmox1a
ugt1b1
fth1a
fthl28
fthl30
hamp
slc11a2
slc25a37
slc25a28
slc40a1
tfa
Heme biosynthesis
Heme catabolism
Iron transport, storage & regulation
c
Oxidative stress & AhR signaling-related genes
C
BE
mRNA expression (log2 fold change)
cat
gpx1a
gpx2
gpx3
gpx4
nos2a
nos2b
prdx1
prdx2
prdx3
prdx4
prdx6
sod1
sod2
sod3a
sod3b
txn
ahr2
cyp1a
gstp1
nfe2l2a
nqo1
Oxidative stress, ROS/NOS regulation
AhR signaling
d
FA-supplemented HepaRG cells
C
BE
mRNA expression (log2 fold change)
p=0,068
p=0,056
p=0,061
ABCG2
TSPO
SDHA
UQCC3
ABCB6
ALAS1
FECH
BLVRA
HMOX1
FTH1
SLC11A2
SLC25A37
SLC25A28
SLC40A1
TF
CAT
PRDX1
NFE2L2
NQO1
Transport & metabolism
Respiratory chain
Heme biosynthesis
Heme catabolism
Iron transport, Storage & Regulation
Oxidative stress
AhR signaling

Figure 2

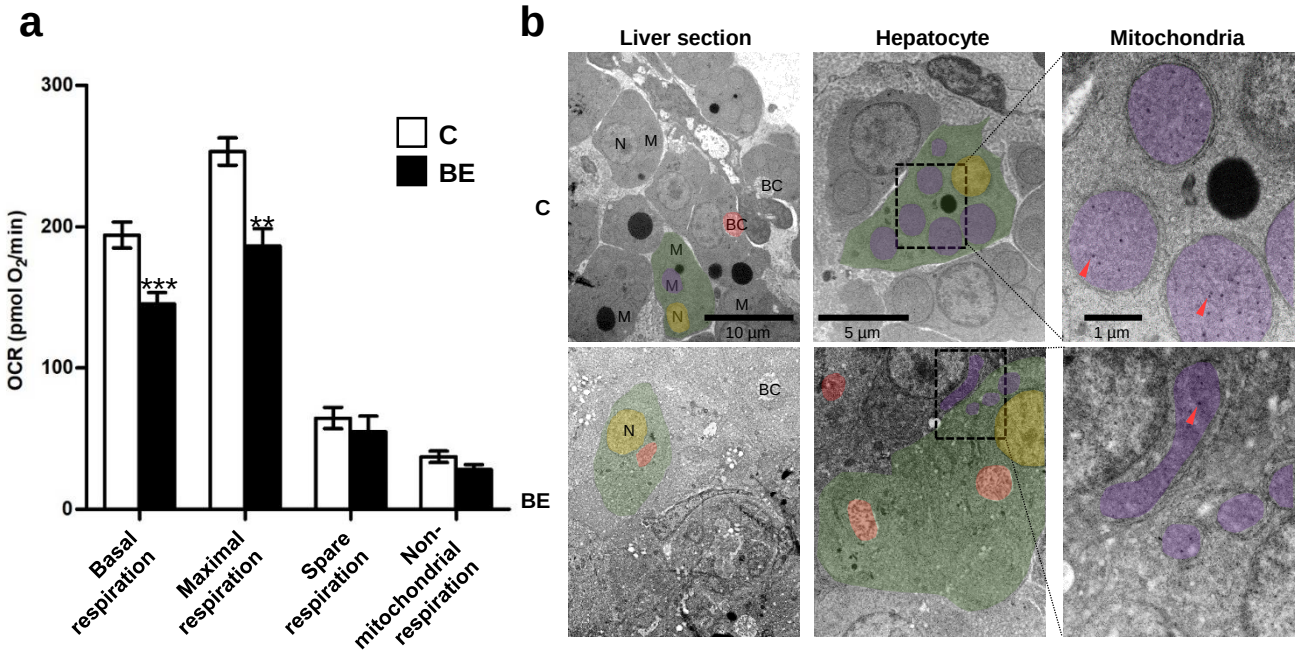
a
300
200
100
0
OCR (pmol O2/min)
C
BE
***
**
Basal respiration
Maximal respiration
Spare respiration
Non-mitochondrial respiration
b
Liver section
Hepatocyte
Mitochondria
C
BE
N
M
BC
10 µm
5 µm
1 µm

Figure 3

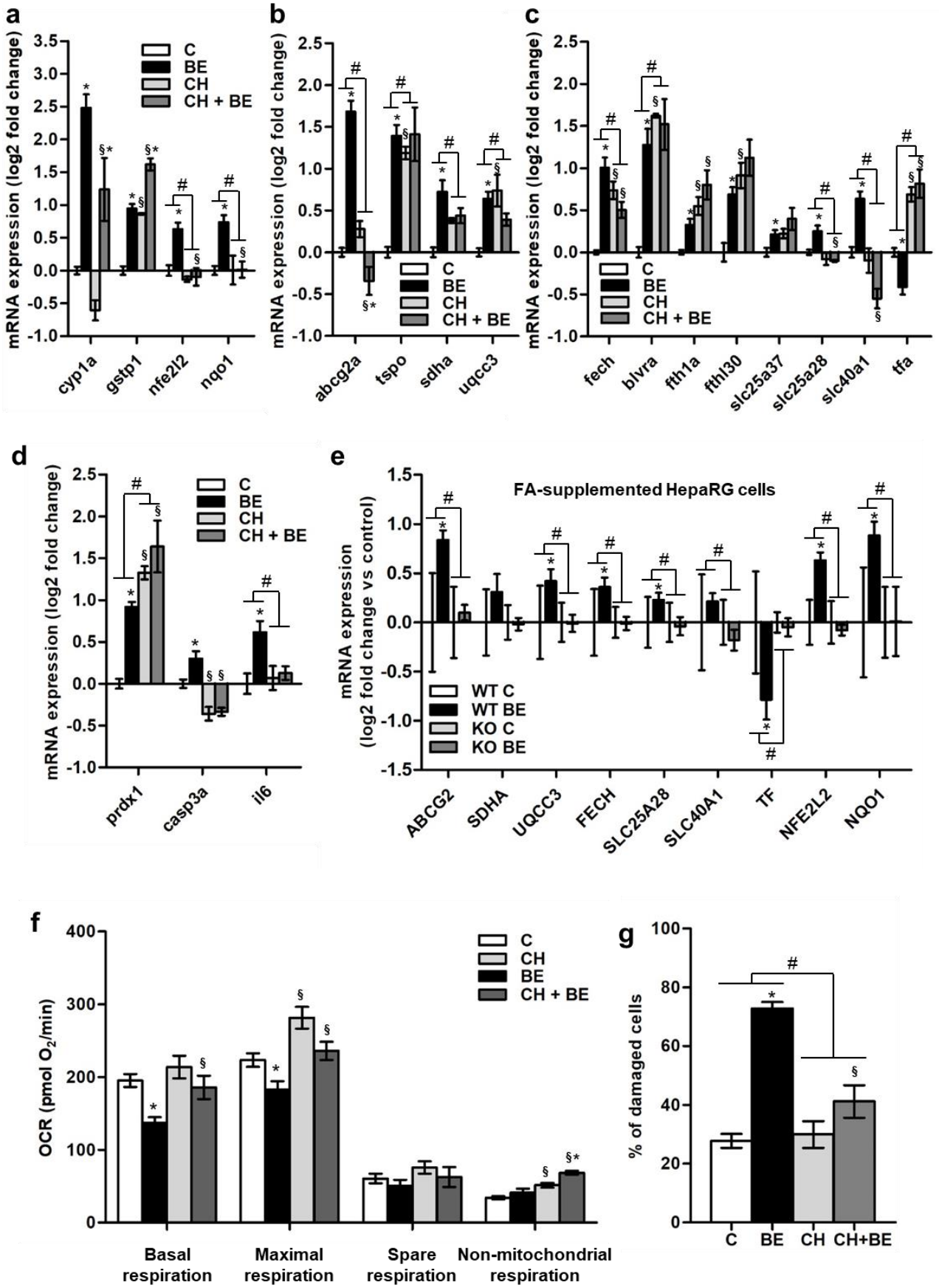
a
b
c
mRNA expression (log2 fold change)
C
BE
CH
CH + BE
cyp1a
gstp1
nfe2l2
nqo1
abcg2a
tspo
sdha
uqcc3
fech
blvra
fth1a
fthl30
slc25a37
slc25a28
slc40a1
tfa
d
e
prdx1
casp3a
il6
FA-supplemented HepaRG cells
mRNA expression (log2 fold change vs control)
WT C
WT BE
KO C
KO BE
ABCG2
SDHA
UQCC3
FECH
SLC25A28
SLC40A1
TF
NFE2L2
NQO1
f
g
OCR (pmol O2/min)
Basal respiration
Maximal respiration
Spare respiration
Non-mitochondrial respiration
% of damaged cells
C
BE
CH
CH+BE

Figure 4

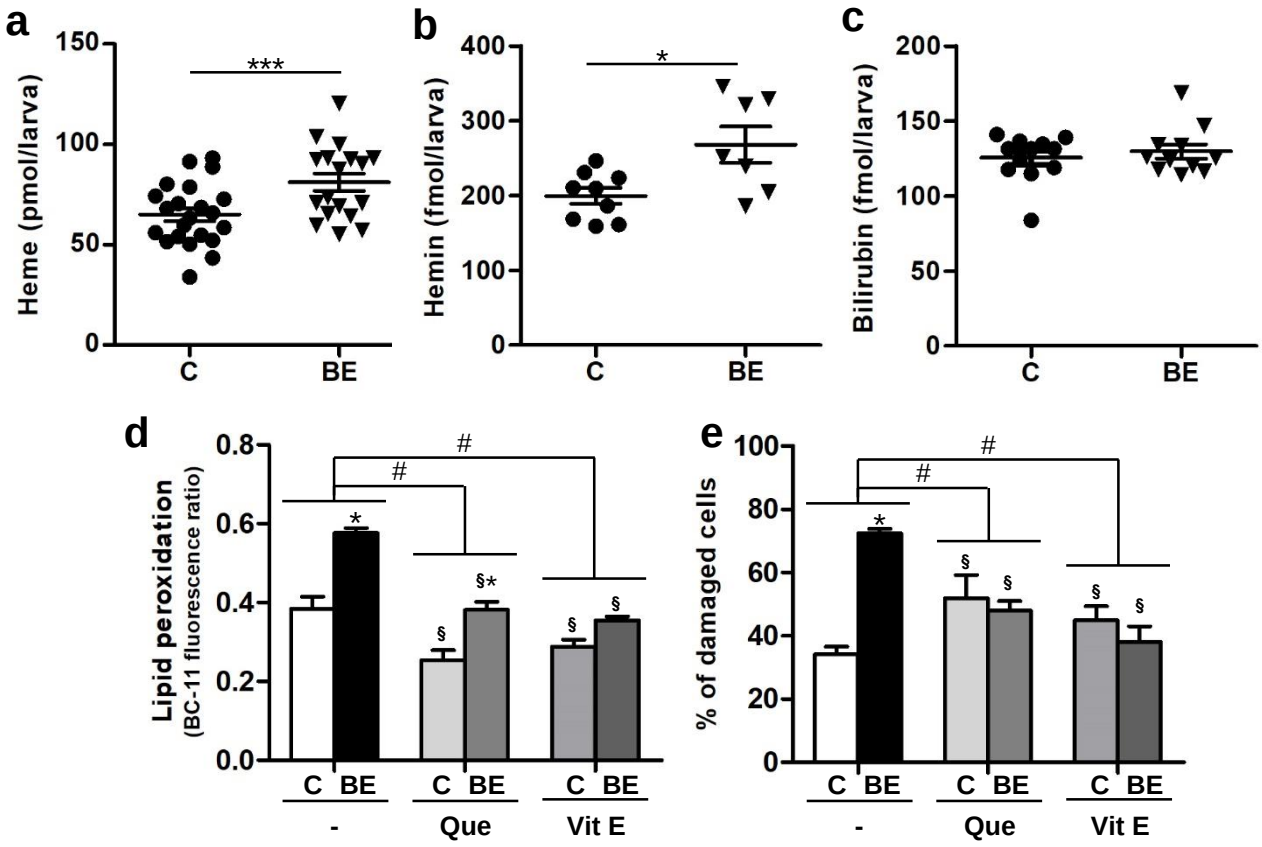
a
Heme (pmol/larva)
150
100
50
0
***
C
BE
b
Hemin (fmol/larva)
400
300
200
100
0
*
C
BE
c
Bilirubin (fmol/larva)
200
150
100
50
0
C
BE
d
Lipid peroxidation
(BC-11 fluorescence ratio)
0.8
0.6
0.4
0.2
0.0
#
#
*
§
§*
§
§
C BE
C BE
C BE
-
Que
Vit E
e
% of damaged cells
100
80
60
40
20
0
#
#
*
§
§
§
§
C BE
C BE
C BE
-
Que
Vit E

Figure 5

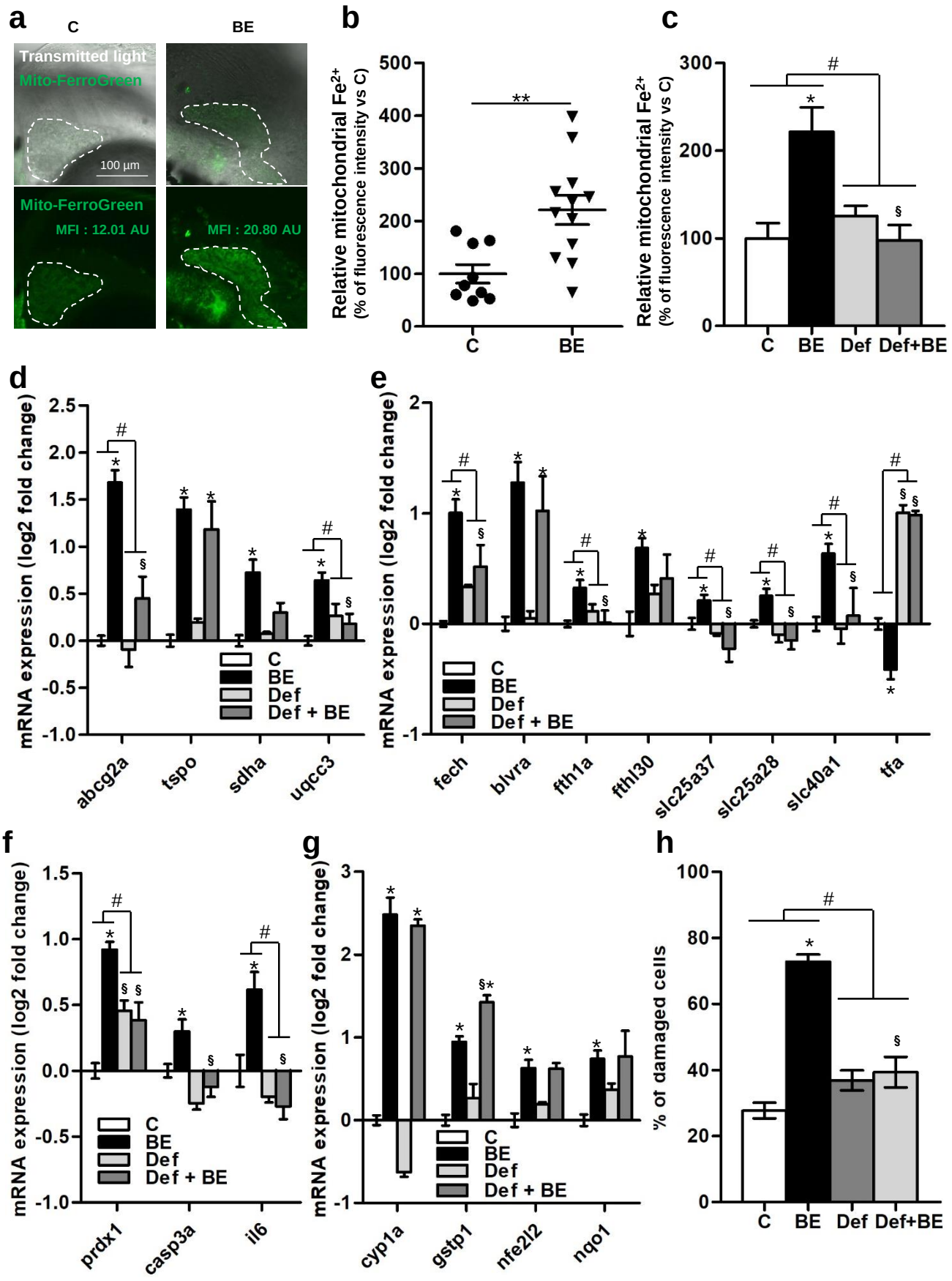
a
C
BE
Transmitted light
Mito-FerroGreen
100 µm
Mito-FerroGreen
MFI : 12.01 AU
MFI : 20.80 AU
b
Relative mitochondrial Fe2+
(% of fluorescence intensity vs C)
**
C
BE
c
Relative mitochondrial Fe2+
(% of fluorescence intensity vs C)
C
BE
Def
Def+BE
d
mRNA expression (log2 fold change)
C
BE
Def
Def + BE
abcg2a
tspo
sdha
uqcc3
e
mRNA expression (log2 fold change)
C
BE
Def
Def + BE
fech
blvra
fth1a
fthl30
slc25a37
slc25a28
slc40a1
tfa
f
mRNA expression (log2 fold change)
C
BE
Def
Def + BE
prdx1
casp3a
il6
g
mRNA expression (log2 fold change)
C
BE
Def
Def + BE
cyp1a
gstp1
nfe2l2
nqo1
h
% of damaged cells
C
BE
Def
Def+BE

Figure 6

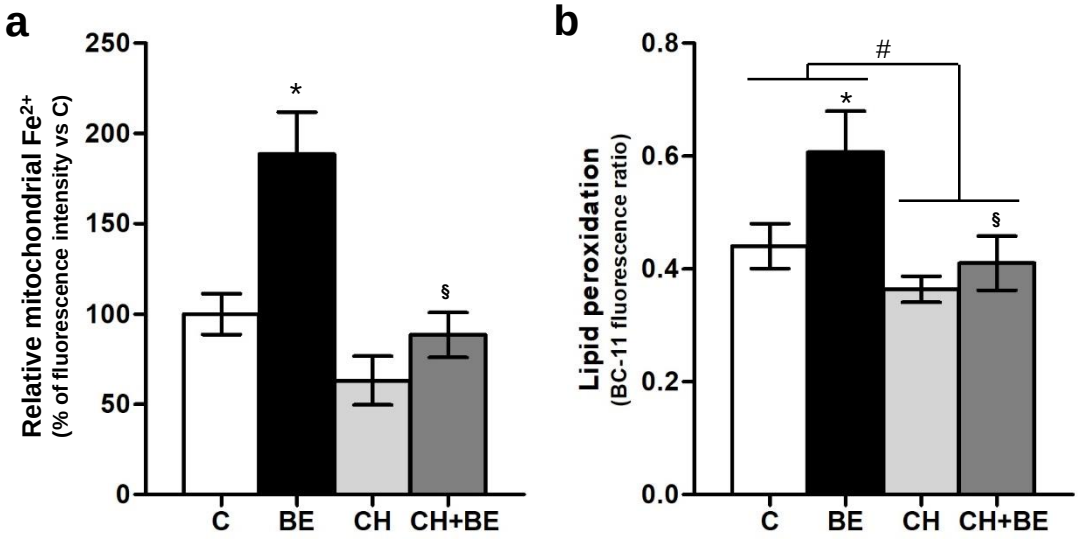
a
Relative mitochondrial Fe2+
(% of fluorescence intensity vs C)
250
200
150
100
50
0
*
§
C
BE
CH
CH+BE
b
Lipid peroxidation
(BC-11 fluorescence ratio)
0.8
0.6
0.4
0.2
0.0
#
*
§
C
BE
CH
CH+BE

Figure 7

Graphical Abstract

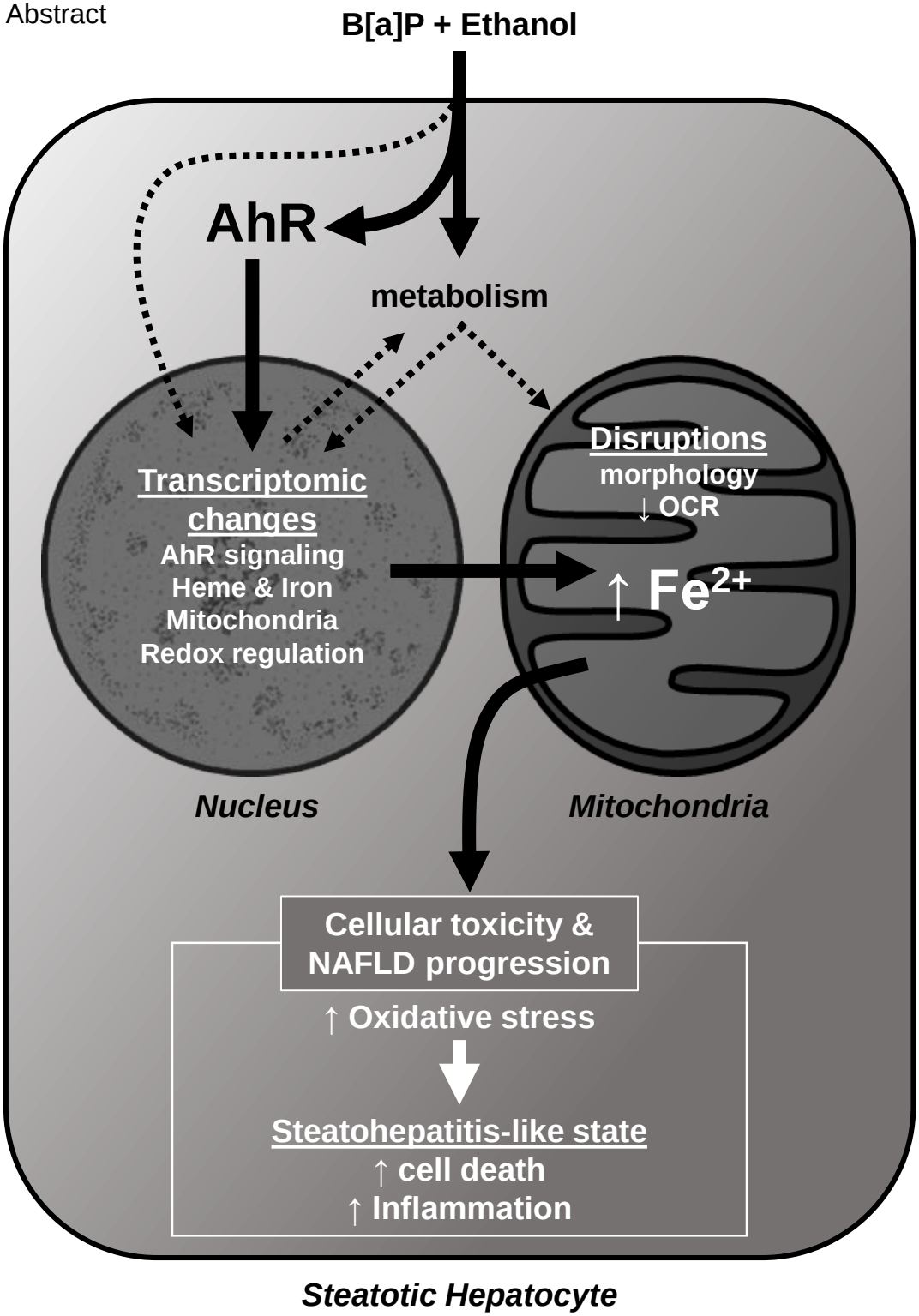

Highlights

- A transcriptomic approach was used on an *in vivo* model of zebrafish larvae to reveal mechanisms of NAFLD progression induced by B[a]P/ethanol co-exposure.
- B[a]P/ethanol co-exposure aggravates NAFLD through mitochondrial dysfunction.
- AhR activation induced by B[a]P/ethanol co-exposure is responsible of mitochondrial iron overload and oxidative stress involved in toxicant-induced NAFLD progression.